DISTINGUISHED PAPERS

MIST, Dhaka, Bangladesh, 14–15 December 2015

DRIVE-BY BRIDGE DAMAGE DETECTION USING APPARENT PROFILE

Ahmed El-Hattab[1], Nasim UDDIN[2] and Eugene Obrien[3]

[1, 2] University of Alabama at Birmingham

[3] University College Dublin, Ireland

Abstract. *Bridge structures are subjected to continuous degradation due to environmental effect and excess loading. Monitoring of bridges is a key part of any maintenance strategy as it can give an early warning if the bridge becomes unsafe. This paper theoretically assesses the ability of vehicle fitted with accelerometers to detect damage in the bridge. Damage is defined in this study as change in damping ration and loss in structure stiffness. Two car models are used in this investigation. The first is the two degree of freedom quarter car model, while the second is four degree of freedom half car model. The bridge is modeled as a simply supported beam. Both car and bridge are modeled using Finite Element Analysis LS-DYNA program. Both smooth and rough profiles are used in the study.*

Keywords: Bridge structure, Degradation, Damage, Finite element analysis.

1   INTRODUCTION

In recent years there has been a move toward sensor based monitoring for bridges instead of visual inspection. However, sensor base monitoring is costly, and need maintenance. Some authors have shifted to the instrumentation of a passing vehicle, rather than the bridge for monitoring. This approach is referred to as 'drive-by' bridge inspection (Kim and Kawatani, 2009). Using this approach, bridge itself is not instrumented, and so the concept has the potential to be far more cost effective than traditional Structure Health Monitoring.

The feasibility of using an instrumented vehicle to extract the first natural frequency of the bridge has been verified in numerical studies and filed tests (Yang et al., 2004; Lin and Yang, 2005; Oshima et al., 2008). The use of drive-by method for health monitoring has been developed by Kim and Kawatani (2009), McGetrick et al. (2010) and Toshinami et al. (2010).

McGetrick et al. (2009) investigated the effect of road profile on drive-by methods for health monitor. Results show that the method works well in absence of road roughness, that the road roughnessexcites the bridge and the axle frequency acceleration become predominate in the Power Spectral Density.

Keenahan et al. (2012) studied the use of half car four degree of freedom system (with two axles) model over rough profile. The study shows that the effect of road profile in acceleration spectra can be removed by subtracting the two axle acceleration at the same location.

This paper presents a novel alternative to acceleration signal analysis using the Apparent Profile to detect bridge damage. When a car passes over certain profile without a bridge, the car starts to excite. Using the acceleration data as an input we can recalculate the profile that causes the excitation. If the car starts to pass over the same profile with healthy bridge, the back calculated profile will be contaminated by bridge displacement which refers to the 'Apparent Profile'. By repeating the process for the same road profile with damaged bridge we will have a damaged 'Apparent Profile'. Subtracting the damaged apparent profile from undamaged one will show the damage level of the bridge.

2   VEHICLE AND BRIDGE MODEL

Two different car models are used in this paper for the car. The First one is the theoretical quarter car model (Fig. 1) with two degree of freedom, which allows for axle hop and body mass bouncing. The body mass of the car is presented by a suspension mass ms while the axle mass is presented by ma. The body mass ms is connected to the axel mass ma by a suspension spring with stiffness ks and viscous damper with damping value cs. The axel mass is connected to the road surface by spring with stiffness ka. The tire damping has been neglected. The

body mass vertical acceleration is represented by $\ddot{u}_s$ and the axle vertical acceleration is represented by $\ddot{u}_a$
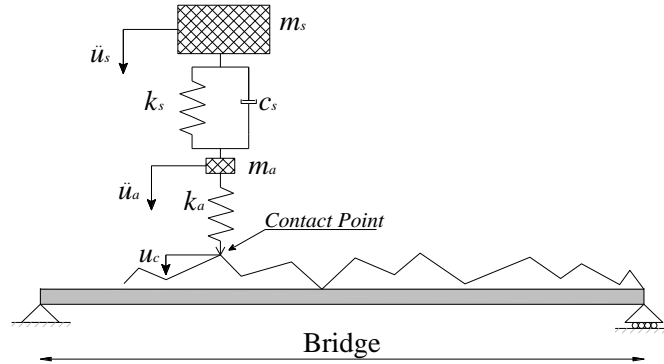

Figure 1: Theoretical quarter car model

The properties of the car are listed in Table 1 and are obtained from work by Cebon(1999) and Harrise et al.(2007)

Table 1: properties of quarter car model

Property	Unit	Symbol	Quarter Car Model
Body Mass	kg	ms	17300
Axel Mass	kg	ma	700
Suspension Stiffness	N/m	ks	4 × 105
Suspension Damping	N.s/m	cs	10 × 103
Tire Stiffness	N/m	ka	1.75 × 106
Body mass frequency of vibration	Hz	fbounce	0.69
Axel mass frequency of vibration	Hz	faxle	8.8

The second model is for the theoretical half car model (Fig. 2) with four degree of freedom, which allows for axle hop, body mass bouncing and body mass pitch rotation which is not available in the quarter car model. The body mass is presented as ms, while the axle mass as ma1, ma2 for axle 1 and 2 respectively. The body mass is connected to the axle mass by a spring with stiffness ks1, ks2 and with viscous damper cs1, cs2 for axle 1 and 2 respectively. The axle mass is connected to the road surface by spring with stiffness ka1, ka2.The tier damping has been neglected for this model too. The body mass represented in LS-DYNA as a rigid bar with mass moment of inertia Is, to account for the body mass pitch rotation. The distance between each axel to the body mass center of gravity is D1

& D2 for axle 1 and 2 respectively. In this case the body mass center of gravity is considered in the middle between the two axles (D1= D2).
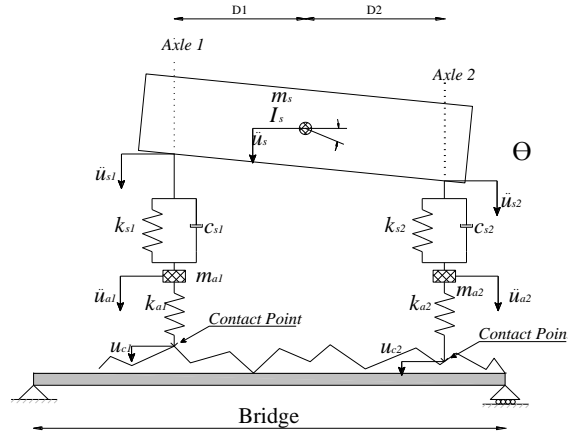

Figure 2: Theoretical half car model

The properties of the half car are listed in Table 2 and are based from work by Cebon(1999) and Harrise et al.(2007).

Table 2 properties of quarter car model

Property	Unit	Symbol	Quarter Car Model
Body Mass	kg	ms	16600
Axel Mass	kg	ma1,ma2	700
Suspension Stiffness	N/m	ks1,ks1	4×10^5
Suspension Damping	N.s/m	cs1,cs2	10×10^3
Tire Stiffness	N/m	ka1,ka2	1.75×10^6
Mass moment of Inertia	kg.m2	Is	95765
Distance of axle to center of gravity	m	D1,D2	2.375
Body mass frequency of vibration	Hz	fbounce	1
		fpitch	1
Axel mass frequency of vibration	Hz	faxle1, faxle2	8.8

In this paper we studied three different real bridges with 10 m, 20 m and 30m spans. The three bridges properties have been calculated from the geometry of the bridges. An Eigen value analysis has been made to extract the bridges first natural frequencies. The three bridge properties are listed in Table 3

Table 3 properties of Actual Bridges

Bridge(m)	First Natural Frequency (Hz)	Moment of inertia around horizontal axe (m4)
10	8.75	0.0434
20	3.77	0.1518
30	2.39	0.3534

An equivalent 1D Belytschko-Schwer full cross-section integration beam element is used to represent the three bridges. The equivalent rectangular beam has the same moment of inertia and first natural frequency for the three bridges. All three bridges have Elastic Modulus of Ec=3.5 × 1010 N/m2 and density of γ=2400 kg/m3. The equivalent Bridges properties are listed in Table 4

Table 4 Equivalent 1D bridge properties

Bridge	First Natural Frequency(Hz)	Moment of inertia around horizontal axe (m4)	Section Area(m2)
10m	8.75	0.0434	2.04
20m	3.77	0.1518	2.40
30m	2.39	0.3534	2.76

The crossing of the moving vehicle over the bridge is modeled by LS-DYNA FEA program. Both quarter and half car model are used to move with 25m/s constant speed over a 200 m approach distance to reach the steady state case for car excitation, followed by the bridge. The quarter car used to move over both smooth and rough road profiles, while the half car model simulated passing over rough profile only for the sake of the brevity of the paper.
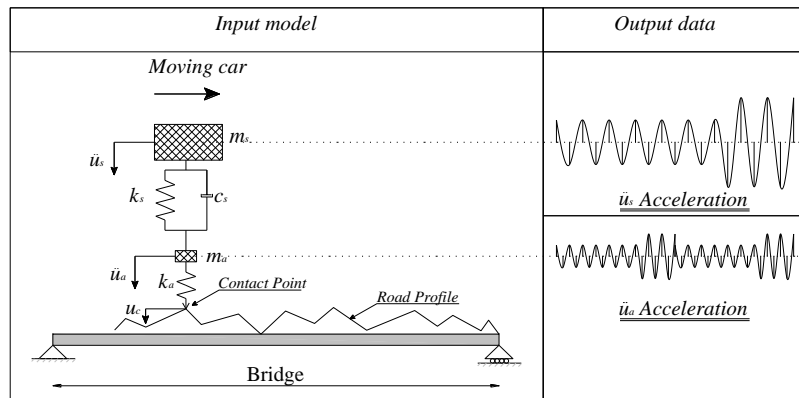
3   CALCULATION OF THE APPARENT PROFILE

This section describes the Apparent Profile calculation process for quarter car model . The process is divided into two main stages, both of them are used to be modeled using LS-Dyna FEA program. First to run the quarter car model over the bridge to generate the acceleration data for the body mass $\ddot{u}_s$ and the axle mass $\ddot{u}_a$. This model use to simulate the actual acceleration data that will be collected from the instrumented truck. The quarter car applies a force on the bridge which can be calculated form equation (1)

$$F = m_s.\ddot{u}_s + m_a.\ddot{u}_a + (m_s + m_a).g \qquad (1)$$

Where 'g' is the ground acceleration. This force will be used as a data input in the second model to get the apparent profile.

The second model is for quarter car only without bridge. By applying the body mass acceleration $\ddot{u}_s$ to the body mass, the axle mass acceleration $\ddot{u}_a$ to the axle mass and the force 'F' to the contact point, then running this model we should get the same profile 'u_c' which produce the acceleration data. The method is illustrated in Fig. 3

a)First Model : simulate the real life truck and the accelerometer data.
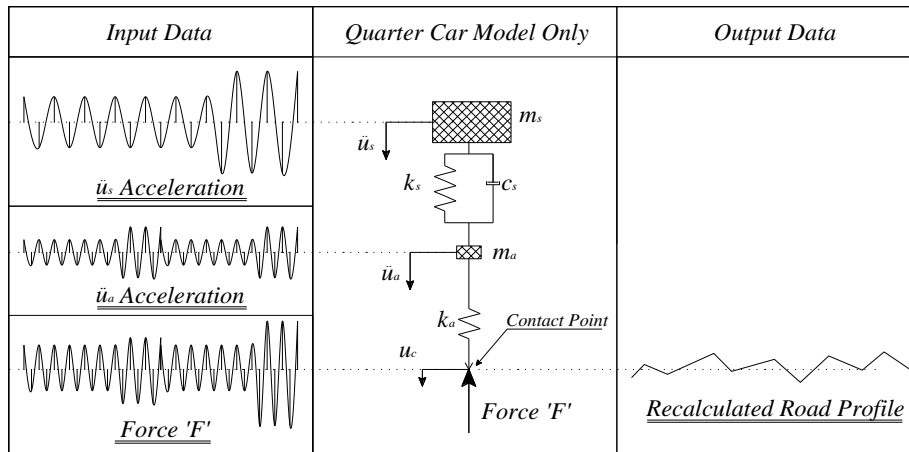

b)Second Model : recalculatingthe profile u_c

Figure 3: Apparent Profile calculation process

4   RESULTS OF QUARTER CAR OVER BRIDGE WITHOUT ROAD ROUGHNESS

In this section, the quarter car is simulated crossing a approach distance followed by damaged bridge. The damages are modeled with two criteria, first as change in damping as since it shows to be quite sensitive for structural damage (Curadelli et al. 2008). Second as loss in stiffness as recommended by Shinha et al. (2002). The crack cause a loss in stiffness over a region of three times the beam depth varying linearly from maximum at the center. The damage is defined as ration of crack depth to over all beam depth; thus, 20% damage implies that the crack depth is 20% of the beam depth. The crack used to be molded at one third of the beam length for the three bridges.

The quarter car crosses a 200 m approach distance followed by 10m simply supported bridge. This is repeated six times one for each damping ratio (from 0% to 5%). The process is repeated again six times for each damage level (from 0% to 50%).

The quarter car axel acceleration is transformed from the time domain to the frequency domain using the fast Fourier transform (FFT). The sampling rate of the data is 1000 Hz, the length of the acceleration signal is 400 samples, the frequency resolution is 2.5Hz. The six different power spectral density (PSD) curves are plotted on the same graph for each damage criteria, with frequency in x-axis, and can be seen in Fig. 4. Peak in the acceleration spectra can be seen near the bridge frequency (8.75 Hz) for both damage criteria. However, for change in damping a decrease in the PSD peak can be seen as the bridge damping increase, but for lose in stiffness almost no change in the PSD peak. The process has been made for the 20 m and 30 m bridge too and they give the same results so they are not included in the paper.
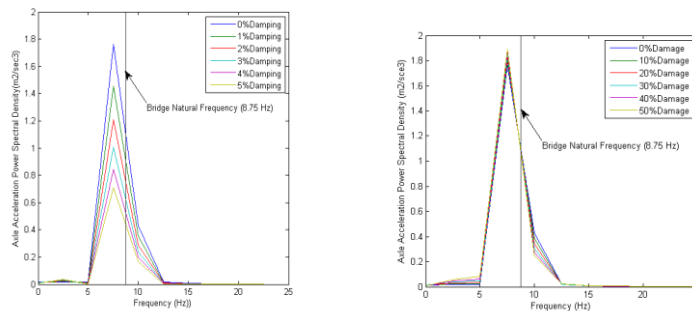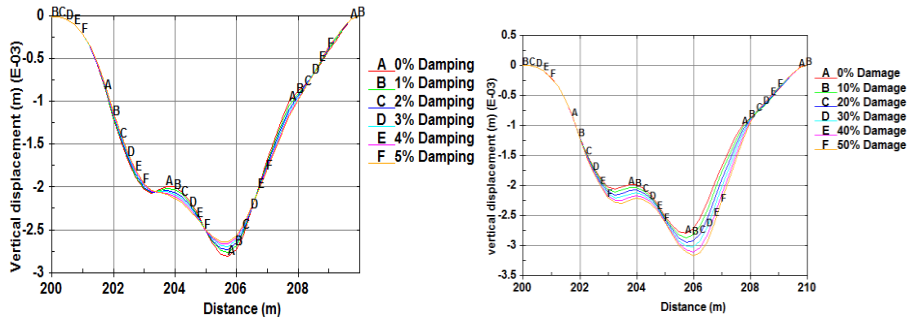

a) For change in Damping   b) For change in Stiffness
Figure 4 PSD for axle acceleration for 10 m bridge with no roughness

Using the body mass acceleration $\ddot{u}_s$ and the axle acceleration $\ddot{u}_a$ from the quarter car model and applying in equation (1) to get force 'F', then applying

$\ddot{u}_s, \ddot{u}_a$ and the force 'F' as an input in the quarter car model only (without bridge) the profile 'u_c' is recalculated which refers to the Apparent Profile. This process is repeated twelve times for damping ration from 0% to 5%, and for damage from 0% to 50%. The six different Apparent Profile curves are plotted on the same graph for each damage criteria with distance in x-axis, and can be seen in Fig. 5.
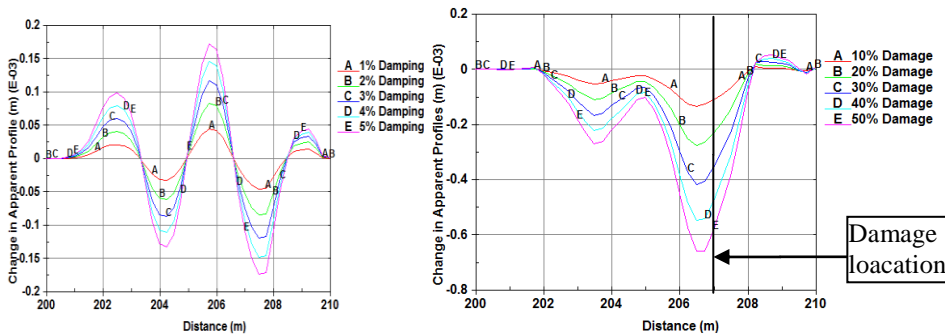

a) For change in Damping   b) For change in Stiffness

Figure 5: Apparent Profile for quarter car model for 10 m bridge with no roughness

The change in the Apparent Profile represent the damage level in the bridge, so damage level for 1% damping can be calculated by subtracting the Apparent Profile for 1% damping from the Apparent Profile for 0%. For 2% damping, by subtracting the Apparent Profile for 2% damping from the Apparent Profile for 0% and so on. A plot shows the difference between Apparent Profiles for each damage level is shown in Fig.6 for both damage criteria. From Fig. 6 the Apparent Profile shows to be very sensitive for damage for both adopted criteria unlike the PSD. Also it can be used for damage localization since they show a higher displacement at the location of damage as shown in Fig. 6b. The process has been made for the 20 m and 30 m bridge too and they give the same results so they are not included in the paper.


a) For change in Damping   b) For change in Stiffness

Figure 6: Change in Apparent Profile for 10 m bridge with no roughness

5   RESULTS OF QUARTER CAR OVER BRIDGE WITH ROAD ROUGHNESS

In this section, a rough profile is included in the in the simulation. The road roughness is randomly generated according to ISO (International Organization for Standardization). Road roughness Class 'A' used for a 'very good' profile (Fig. 7a) and Class 'B' for 'good' profile (Fig. 7b).
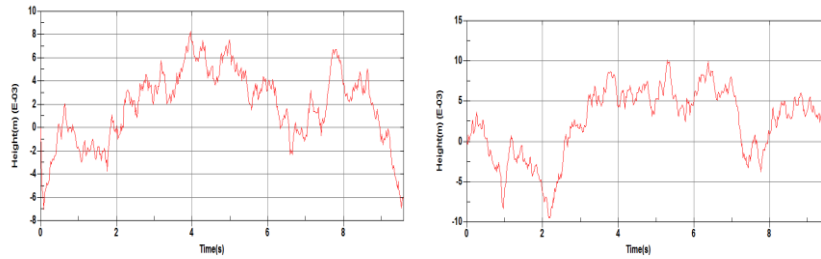

a) Road profile Class 'A'   b) Road profile Class 'B'
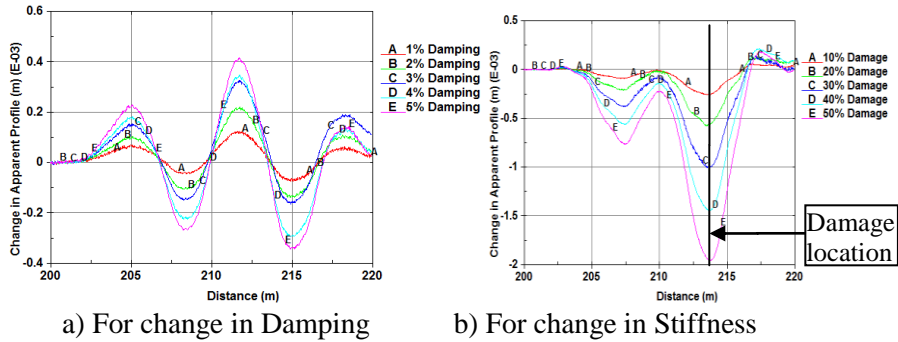Figure 7 Road profile Class 'A' & 'B' with respect to time

The quarter cross a 200 m approach distance followed by 20m simply supported bridge with road roughness Class 'B'. This is repeated six times one for each damping ratio (from 0% to 5%). The process repeated again six times for each damage level (from 0% to 50%).

The quarter car axel acceleration is transformed from the time domain to the frequency domain using the fast Fourier transform (FFT). The sampling rate of the data is 1000 Hz, the length of the acceleration signal is 800 samples, the frequency resolution is 1.25Hz. The six different power spectral density (PSD) curves are plotted on the same graph for each damage criteria, with frequency in x-axis, and can be seen in Fig. 8. Peak in the acceleration spectra can be seen near the axel frequency (8.8 Hz) for both damage criteria and almost no difference is observed between each damage level. The process has been repeated for road roughness Class 'A' and it shows the same results so they are not included the paper. The process has been made also for the 30 m bridge and it gives the same results so they are not included in the paper (for 10 m bridge it has been removed that it shows a resonance case since fbridge =8.75Hz).

The Apparent Profile has been extracted using the same process. A plot shows the difference between Apparent Profiles for each damage level is shown in Fig.9 for both damage criteria. As shown the Apparent profile still detects the damage, and it is not affected by the road roughness.
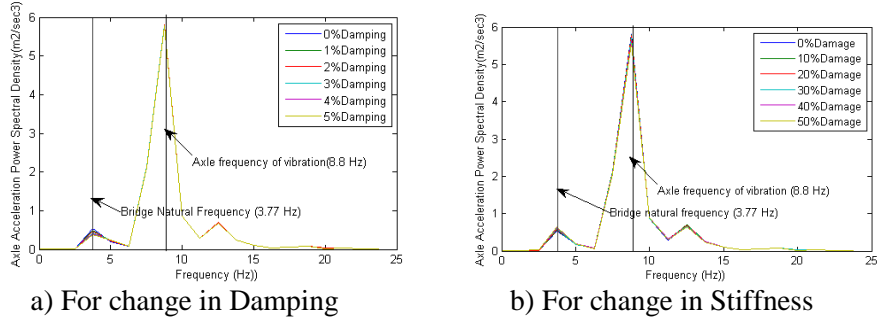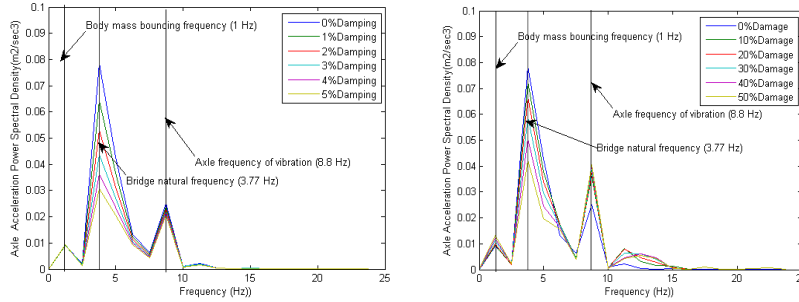
a) For change in Damping   b) For change in Stiffness

Figure 8: PSD for axle acceleration for 20 m bridge with roughness Class 'B'

a) For change in Damping   b) For change in Stiffness

Figure 9: Change in Apparent Profile for 20 m bridge with roughness Class 'B'

6   RESULTS OF HALF CAR OVER BRIDGE WITH ROAD ROUGHNESS

Keenahanet al (2012) recommended using a half car model to remove the effect of car bouncing. By subtracting Axle 1 acceleration from Axles 2 acceleration when it reach the same location of Axle 1(in our case with time shift of 0.19 sec) the bouncing effect of the car should be removed. The half car cross a 200 m approach distance followed by 20m simply supported bridge with road roughness Class 'A'. This is repeated six times one for each damping ratio (from 0% to 5%). The process repeated again six times for each damage level (from 0% to 50%). The subtracted axel acceleration is transformed from the time domain to the frequency domain to get PSD. The six different power spectral density (PSD) curves are plotted on the same graph for each damage criteria, with frequency in x-axis, and can be seen in Fig. 10. The PSD shows to detect the damage for both cases, however the axle frequency of vibration and body mass pitching frequency still have effect in the PSD. It is expected that this effect is not significant here since the mass in the middle between the two axles and should be higher if the body mass is not in the middle.
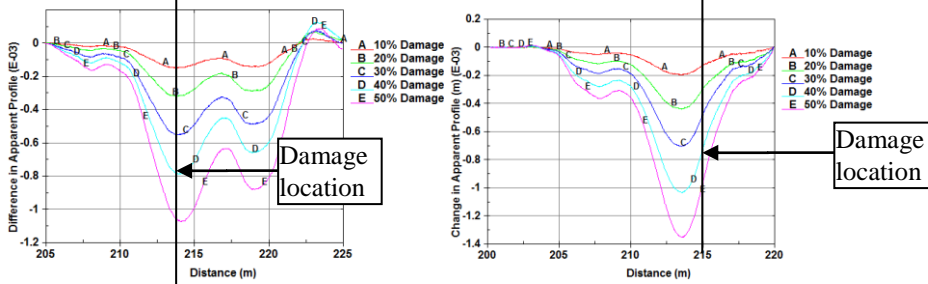
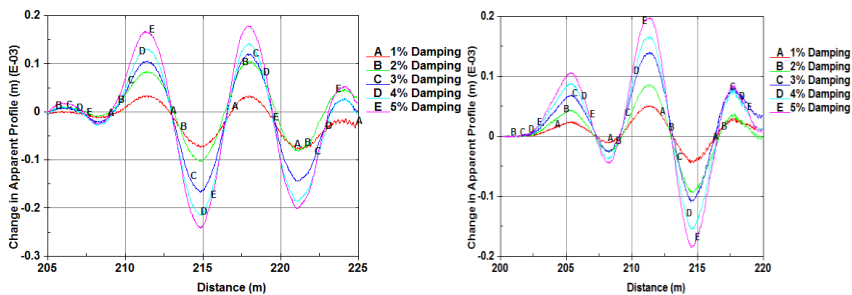a) For change in Damping   b) For change in Stiffness

Figure 10: PSD for subtracted axle acceleration for 20 m bridge with roughness Class 'A'

The Apparent Profile has been extracted using the same process for the two axles. A plot shows the difference between Apparent Profiles for each damage level is shown in Fig.11 for both damage criteria. As shown the Apparent Profile still detect the damage properly for the two damage criteria for the two axles. Also the damage location can be detected and it is in the same location for the Apparent Profile of Axle 1 and Axle 2.

a) Apparent Profile for Axle   b) Apparent Profile for Axle 2
for change in stiffness   for change in stiffness

c) Apparent Profile for Axle 1   d) Apparent Profile for Axle 2
for change in damping   for change in damping

Fig. 11 Apparent Profile for half car model for 20 m bridge with roughness Class 'A'

7   CONCLUSION

This study has investigated the feasibility of using the Apparent Profile as a damage indicator instead of the PSD of axle acceleration. The results show that it is possible to detect bridge damage using the Apparent Profile for smooth and rough road. The results also show that the Apparent profile concept can be used for damage localization for the bridge. The PSD results for half car model shows to detect the bridge damage well, however this study didn't consider unsymmetric half car which expected to have higher effect for pitching which may mask the difference for each damage level.

REFERENCES

[1] Kim, C.W. & Kawatani, M. Challenge for a drive-by bridge inspection. Proceedings of the 10th International Conference on Structural Safety and Reliability, ICOSSAR2009. Osaka, Japan. 2009:758-765.

[2] Yang, Y.B., Lin, C.W. & Yau, J.D., 2004. Extracting bridge frequencies from the dynamic response of a passing vehicle. Journal of Sound and Vibration, 272(3-5), pp.471–493.

[3] Lin, C.W. & Yang, Y.B., 2005. Use of a passing vehicle to scan the fundamental bridge frequencies: an experimental verification. Engineering Structures, 27(13), pp.1865–1878.

[4] Oshima, Y., Yamaguchi, T., Kobayashi, Y. & Sugiura, K., 2008. Eigen frequency estimation for bridges using the response of a passing vehicle with excitation system. In Proceedings of the Fourth International Conference on Bridge Maintenance, Safety and Management, IABMAS2008. Seoul, Korea: CRC Press, Taylor and Francis Group, London, UK, pp. 3030–3037.

[5] McGetrick, P.J., González, A. & O'Brien, E., 2010. Monitoring bridge dynamic behaviour using an instrumented two axle vehicle. In Bridge and Concrete Research in Ireland. Cork, Ireland.

[6] Toshinami, T., Kawatani, M. & Kim, C.W., 2010. Feasibility investigation for identifying bridge's fundamental frequencies from vehicle vibrations. In Proceedings of the Fifth International Conference on Bridge Maintenance, Safety and Management, 20 IABMAS2010. Philadelphia, USA: CRC Press, Taylor and Francis Group, London, UK, pp. 317–322.

[7] McGetrick, P.J., González, A. & OBrien, E.J., 2009. Theoretical investigation of the use of a moving vehicle to identify bridge dynamic parameters. Insight: Non-Destructive Testing & Condition Monitoring, 51, pp.433–438

[8] Keenahan J., McGetrick P., González, A. & OBrien, E.J., 2012. Using Instrumented Vehicle To Detect Damage In Bridges. Proceedings of 15th International Conference on Experimental Mechanics,2934

[9] Cebon, D. Handbook of vehicle-road interaction. The Netherlands: Swets&Zeitlinger, 1999

[10] Harris, N. K., OBrien, E.J. & González, A., 2007. Reduction of bridge dynamic amplification through adjustment of vehicle suspension damping. Journal of Sound and Vibration, 302: 471-485.

[11] Curadelli, R.O., Riera, J.D., Ambrosini, D. & Amani, M.G., 2008. Damage detection by means of structural damping identification. Engineering Structures, 30:3497-3504.

[12] Sinha JK, Friswell MI and Edwards S., 2002. Simplified models for the location of cracks in beam structures using measured vibration data. J Sound Vib , 251: 13–38.

SEISMIC HAZARD ASSESSMENT FOR BANGLADESH - OLD AND NEW PERSPECTIVES

Tahmeed M. AL-HUSSAINI[1], **Ishika N. Chowdhury**[2] **and Md. N. A. Noman**[3]

[1, 2] BUET-Japan Institute of Disaster Prevention and Urban Safety, Dhaka, Bangladesh
[1, 3] Department of Civil Engineering, Bangladesh University of Engineering and Technology, Dhaka, Bangladesh
Email: [1]htahmeed@yahoo.com, [2]ishika@jidpus.buet.ac.bd and
[3]nayeemnoman@gmail.com

Abstract. *Systematic studies for seismic hazard and risk assessment specifically for Bangladesh have been conducted at a limited scale since early 1990's. This paper attempts to give a brief account of such studies. Research results from seismic hazard studies conducted in recent years by the authors have been presented. Standard probabilistic seismic hazard assessment (PSHA) method has been applied for Bangladesh which is based on earthquake catalogues and available studies on earthquake recurrence intervals. In addition, some neo-deterministic seismic hazard assessment (NDSHA) studies, conducted in collaboration with University of Trieste, have been carried out for scenario earthquakes. Historical earthquakes have been considered as well as earthquakes in new locations or potential known faults indicated in recent seismological studies. Reference will be made to the 1993 Bangladesh National Building code and proposed Updated Bangladesh National Building code.*

Keywords: Seismicity in Bangladesh, Probabilistic seismic hazard assessment, Neo-deterministic seismic hazard assessment, Building code

1   INTRODUCTION

The collision of the Indian plate with the Eurasian plate is the cause of frequent earthquakes in the region comprising North-East India, Nepal, Myanmar, Bhutan and Bangladesh. Historically Bangladesh has been affected by large earthquakes with magnitude 7.0 or greater, some of them had their epicenters within the country. Absence of strong earthquakes affecting Bangladesh for more than 80 years has left the current generation unaware of the possibility of a strong earthquake. As a natural consequence, a majority of buildings in the urban areas of Bangladesh are lacking earthquake resistant design. The effect may be further compounded by poor quality of materials and construction. Recurrence of similar earthquakes can therefore cause catastrophic consequences in densely populated urban areas of Bangladesh. Even moderate earthquakes close to the urban cities can cause great havoc. There is a general consensus among national and international experts about the possibility of a large magnitude earthquake occurring in the region any time, due to stress buildup in fault systems caused by the northward movement of the Indian Plate. Assessment of seismic risk is a top priority for the country. Seismic hazard assessment is the first step for the risk assessment, and mitigation measures to be taken depend on the level of hazard estimated.

Standard seismic hazard assessment methods typically follow the following approaches: (i) probabilistic seismic hazard assessment (PSHA) (ii) deterministic seismic hazard assessment (DSHA) (iii) neo-deterministic seismic hazard assessment (NDSHA). In the probabilistic approach, the ground motion at a site is determined in a probabilistic sense considering the possibility of earthquakes of varying magnitude and at different distances affecting the site. On the other hand, the deterministic approach is based on determining the ground motion at a particular site for an earthquake of fixed magnitude at a known fault. Both PSHA and DSHA use simplified attenuation relationships. NDSHA has similar objectives as DSHA, however it is based on the physics of seismic wave propagation and employs numerical techniques to solve the wave propagation problem.

With a brief introduction to the earthquakes occurring in the region, this paper briefly addresses outcomes from different seismic hazard studies done by other researchers, some of them done at local level while some done on a global scale. It then presents some results from PSHA and NDSHA studies conducted under the first author's supervision and compares them with the seismic zoning map of the National Building Code. In particular, recent results from NDSHA studies have been focused. Some findings from recent and ongoing seismological studies have been considered.

2 EARTHQUAKE OCCURRENCE IN BANGLADESH

2.1 Historical Earthquakes

Historically Bangladesh (Ali and Choudhury, 1994) has been affected by five earthquakes of large magnitude (M) greater than 7.0 (Richter scale) during the 61 year period from 1869 to 1930 (Table 1). Among them, the 8.7 magnitude 1897 Great Indian earthquake (M=8.1 re-estimated by Ambraseys and Bilham, 2003) in Shillong, Assam had an epicentral distance of about 230 km from Dhaka. That powerful earthquake caused extensive damages to masonry buildings in many parts of Bangladesh including Dhaka. The 1885 Bengal earthquake (M=7.0, 170 km from Dhaka) and 1918 Srimongal earthquake (M=7.6, 150 km from Dhaka) had their epicenters within Bangladesh, they caused considerable damage locally. The 1762 Chittagong earthquake, also a local earthquake with estimated magnitude M=7.5 (estimates vary depending on sources), although not well documented, is reported to have caused major landmass changes in the coastline from Chittagong to Myanmar. The epicenter is not well-constrained and likely locations vary from near Chittagong to down the Arakan coast. Large earthquakes in this region have not been occurring for quite a long time (85 years) and significant stress buildup in the faults can lead to a major earthquake taking place.

Table 1. List of Major Historical Earthquakes Affecting Bangladesh

Date	Name	Magnitude (Richter)	Epicentral Distance from Dhaka (km)	Epicentral Distance from Sylhet City (km)	Epicentral Distance from Chittagong (km)
2 April 1762	Chittagong Earthquake	7.5			Uncertain but close to Chittagong
10 Jan. 1869	Cachar Earthquake	7.5	250	70	280
14 July, 1885	Bengal Earthquake	7.0	170	220	350
12 June, 1897	Great Indian Earthquake	8.7	230	80	340
8 July, 1918	Srimongal Earthquake	7.6	150	60	200
2 July, 1930	Dhubri Earthquake	7.1	250	275	415
15 Aug. 1950	Assam Earthquake	8.5	780	580	540

2.2 Recent Earthquakes

During the last two decades, the occurrence and damage caused by a number of earthquakes (magnitude between 4 and 6) inside the country (Al-Hussaini, 2005) or near the country's border, more recently the occurrence of large earthquakes in Sikkim and Nepal has raised the awareness among the general people and the government. The damage has been mainly restricted to rural areas or towns near the epicenter, but there have been some instances of damage in urban areas 50 to 100 km away. An under-construction reinforced concrete frame building collapsed killing several people in the port city of Chittagong due to the Nov. 21, 1997 magnitude 6.0 earthquake at the Bangladesh-Myanmar border. This is a typical example of faulty design and construction, collapse occurring at a very low level of shaking, about 100 km from the epicenter of the earthquake. The July 22, 1999 magnitude 5.1 earthquake with its epicenter very near the island of Moheshkhali, caused extensive damage and collapse of rural mud-walled houses. Concrete column of a cyclone shelter was severely damaged. People reported hearing a loud noise (bang) immediately preceding the earthquake which is possible at locations close to the epicenter. Severe cracking damage to brick masonry buildings and severe damage to mud-walled houses were observed in Kolabunia, Barkal Upazilla due to July 27, 2003 magnitude 5.6 Barkal-Rangamati earthquake. Large crack developed for a long distance along the river, indicative of soil movement toward the river. In Chittagong city, about 90 km away from the epicenter, the earthquake caused ground settlement and cracks in the Public Library building and also damaged an electric transformer. The high frequency of earthquakes occurring in the Chittagong area has caused a good deal of anxiety among the people there.

Dhaka city, located in the central region of Bangladesh can be affected by large magnitude earthquakes occurring at a distance in the major fault zones. Another point of major concern is that there are active faults near the city also. This was realized during the Dec. 19, 2001 magnitude 4+ Dhaka earthquake that caused panic among many city residents. The epicenter was very close to Dhaka city. Frightened people in several high rise buildings rushed down the stairs, as they felt considerable shaking in the upper floors. The location and probable magnitude of a probable earthquake near Dhaka needs to be investigated. In recent large magnitude earthquakes have taken place several hundred kilometers from Bangladesh, namely the 2011 M=6.9 Sikkim earthquake and the 2015 M=7.8 Nepal earthquake. Even then they caused long duration shaking in the capital city and created panic.

3   SEISMIC HAZARD ASSESSMENT STUDIES

A chronological brief literature survey on published seismic hazard assessment studies conducted by other researchers at local and global level is presented here.

The first official seismic hazard-zoning map in the country was published in 1979 by the Geological Survey of Bangladesh prepared by a Committee of Experts on Earthquake Hazard Minimization. As shown in Fig.1, it divides the country into three seismic zones with seismic co-efficients of 0.04g, 0.05g and 0.08g, the north-east zone having the highest coefficient. In the process of development of the country's first building code in 1993 (DDC, 1993a), Kundu (1992) prepared an earthquake catalogue, based on data from Indian Society of Earthquake Technology (ISET) and US National Oceanic and Atmospheric Administration (NOAA). This catalogue was included in the supplementary report (DDC, 1993b) to the 1993 Bangladesh National Building Code (BNBC). The Building Code adopted a revised seismic zoning map (Fig.2) with three seismic zones with zone coefficients representing design peak ground acceleration (PGA) and seismic design procedures following Uniform Building Code (ICBO, 1991).
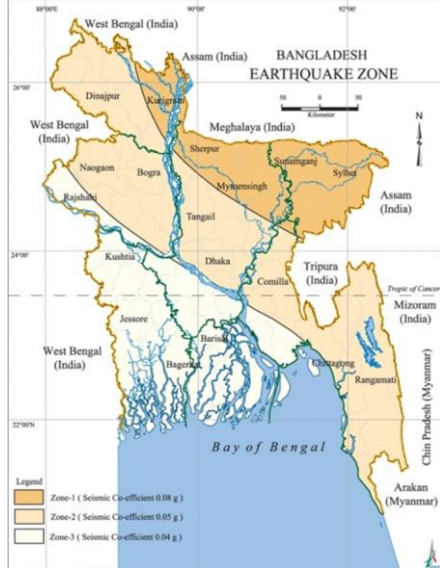

Figure 1: Seismic zoning map in 1993 Bangladesh building code (after Ali and Choudhury,1994)
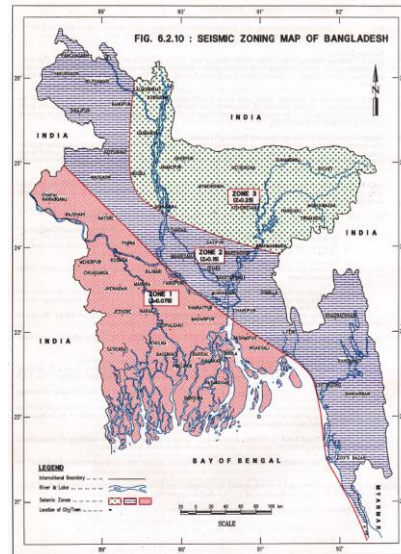
Figure 2: Seismic zoning map in 1993 Bangladesh building code (DDC, 1993)

These zoning coefficients are based on PGA values predicted by Hattori (1979) for a return period of 200 years. This work was done as part of global seismic hazard assessment for different regions by him. Zone 3 lies in the central north and north-east of the country (includes Sylhet, Mymensingh, Jamalpur, Bogra, Kurigram) representing a PGA of 0.25g (Z=0.25). Next to Zone 3 is Zone 2

(which includes the major cities of Dhaka and Chittagong as well as Comilla, Rangpur, Dinajpur, Naogaon) and has a Z value of 0.15. Zone 1 in the south-western part has a Z value of 0.075. Z represents design basis earthquake (DBE).

Global Seismic Hazard Assessment Program (GSHAP) launched in 1992 by the International Lithosphere Program (ILP) performed standard probabilistic seismic hazard assessment works all over the world till 1999. Their predictions for PGA values for a return period of 475 years (10% probability of exceedence in 50 years) are shown in Fig.3. Dhaka appears to have a PGA value of 0.13g, Chittagong 0.24g and Sylhet 0.34g. Ansary and Sharfuddin (2002) formed an earthquake catalogue for the period 1865 to 1995 and used the data for seismic hazard assessment of Bangladesh. They proposed a modified seismic zoning map (Fig.4) with significantly larger areas for Zone 3 and Zone 2, i.e., increased seismic hazard, based on results for return period of 200 years. Their seismic hazard estimation methodology was based on the assumption that the PGA at a site maintains a recurrence frequency relationship [$\log_{10}(PGA)=\alpha-\beta M$, where α, β are regression coefficients] similar to the Gutenberg-Richter magnitude-frequency relationship. The author is of the opinion that this assumption is not generally justified for two reasons. The PGA at a site depends not only on the earthquake magnitude but also on the epicentral distance from the site; in addition different earthquake sources are most likely to possess different frequency characteristics.
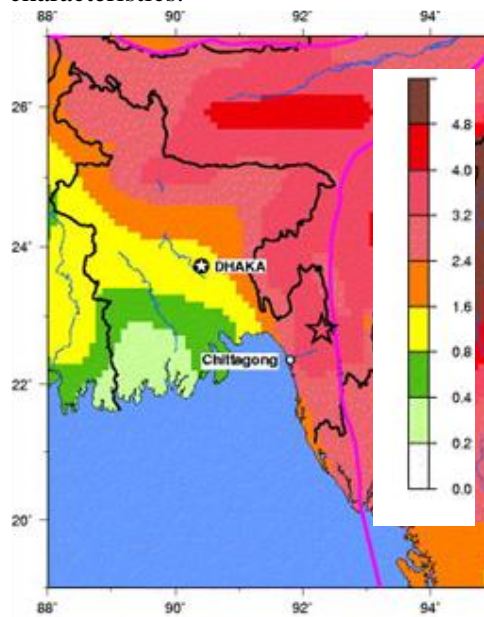

Figure 3: GSHAP Predicted PGA (m/s^2) for return period of 475 years
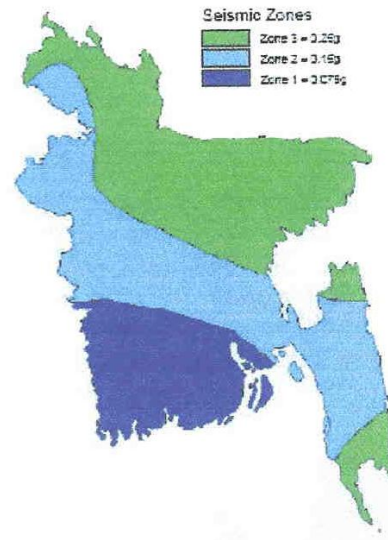

Figure 4: Proposed seismic zoning map (after Ansary and Sharfuddin, 2002)

Noor et al. (2005) presented PSHA results considering rectangular NS oriented seismic sources. Fig.5 presents PGA values for a return period of 475 years. PGA value for Dhaka is around 0.17g, Chittagong 0.2g, Sylhet 0.27g, Mymensingh 0.4g. More recent standard PSHA studies at regional level has been conducted by the National Disaster Management Authority (NDMA), Govt. of India. Fig.6 present NDMA (2010) predicted PGA (in g) for return period of 2475 years. Comparison will be made later with more recent studies which has led to a revised seismic zoning map based on Maximum Considered Earthquake (MCE) and new seismic design criteria for Bangladesh (Al-Hussaini et al., 2012).
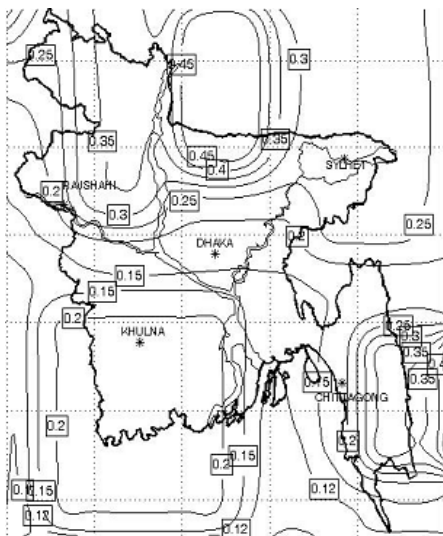

Figure 5: Noor et al. (2005) Predicted PGA (g) for return period of 475 years

Figure 6: NDMA (2010) Predicted PGA (g) for return period of 2475 years

4 DEVELOPMENT OF REVISED SEISMIC ZONING MAP

More recently, standard probabilistic seismic hazard assessment method using multiple source zones has been applied (Al-Hussaini et al., 2012) for determining the PGA values for various return periods ranging from 475 years to 2475 years. The earthquake catalogue has been formed using various sources and including historical earthquakes (Al-Hussaini and Al Noman, 2010). Information from ADPC (2009) work for Comprehensive Disaster Management Program Phase-I has been used. Seismic source zones have been delineated considering Bolt's (1987) source zones in addition to fault locations and cluster of major (M>5) earthquake epicenters affecting Bangladesh. A total of seven seismic source zones have been designated. Four seismic source zone models with some changes in source boundaries have been tried to take into account uncertainties in

source boundaries. The computer program CRISIS (UNAM 1999) is used to perform probabilistic seismic hazard assessment (PSHA) studies for Bangladesh. In the absence of reliable attenuation laws for Bangladesh, recent well-established attenuation relations (one standard deviation above median) developed by various researchers for different regions (Western USA, Eastern USA, Iran, Europe and India) of the world have been used in the study. In addition a new attenuation relationship for Bangladesh originally developed by Islam et al. (2010), and later corrected for site effect, has been used. This local attenuation law is not based on ground motion measurements but is based on intensity based isoseismals of historical and recent earthquakes, and therefore employs intensity-PGA (peak ground acceleration) relationship as well. This law is found to be close to the attenuation law for Western USA developed by Abrahamson and Silva (1997). Bolt (1987) also mentioned that the attenuation in Bangladesh is expected to be similar to that in the Western USA. PSHA results for the attenuation law of Abrahamson and Silva (1997) are presented here.

Recent codes are considering larger return periods to account for large earthquakes with long recurrence periods. The International Building code (ICA, 2006) considers the Maximum Credible Earthquake to correspond to a return period of 2475 years which is equivalent to 2% probability of exceedance in 50 years. The Indian Code (BIS, 2005) is using Maximum Considered Earthquake (MCE) motion in its seismic zoning map.
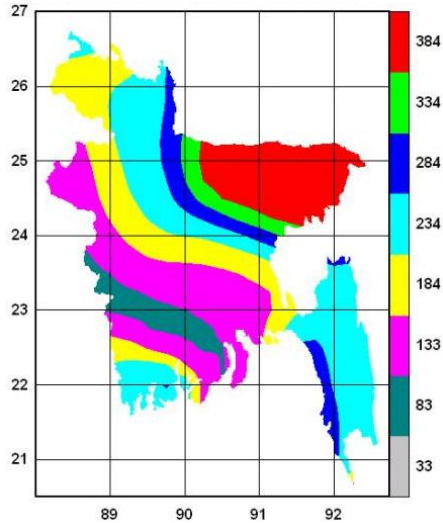

Fig.7 Predicted PGA (cm/sec^2) for return period of 2475 years for source zone model-2 and attenuation law of Abrahamson and Silva, 1997
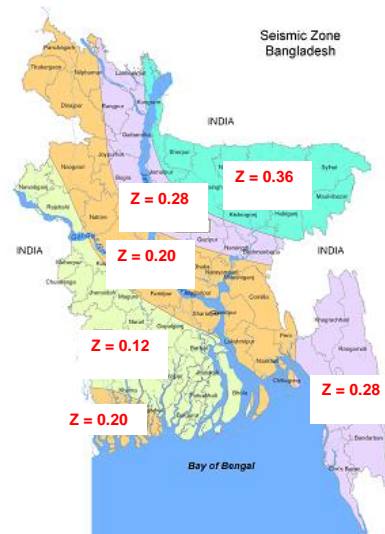

Fig.8 Proposed Seismic Zoning Map for Bangladesh based on Maximum Considered Earthquake (MCE)

Figure 7 shows results of PSHA studies for a return period of 2475 years for seismic source zone model no.2 and using the attenuation law of Abrahamson and Silva (1997). It is observed that the maximum PGA value is 0.38g (g is acceleration due to gravity) in the north and north-east of Bangladesh, the PGA value in Chittagong city is 0.28g, the PGA value in Dhaka city is around 0.18g. These PGA values are for rock or firm soil and do not include local site effect.

New seismic design provisions including a new seismic zoning map has been proposed for the updated Bangladesh national building code (Updated BNBC). The concept of Maximum Considered Earthquake (MCE) with a return period of 2475 years has been introduced. Fig. 8 presents the proposed seismic zoning map for Bangladesh, which is based on the following: (i) PSHA results for return period of 2475 years (ii) limited NDSHA results (iii) effects of large historical earthquakes (iv) previous seismic zoning map of BNBC-1993 (v) new seismic zoning map of neighbouring India and (vi) work of other researchers. The country is divided into four (instead of three) seismic zones with zone coefficient Z equal to 0.12 (Zone 1), 0.2 (Zone 2), 0.28 (Zone 3) and 0.36 (Zone 4). The zone coefficient represents the PGA value for MCE on rock or very stiff soil site. Site effect is not included.
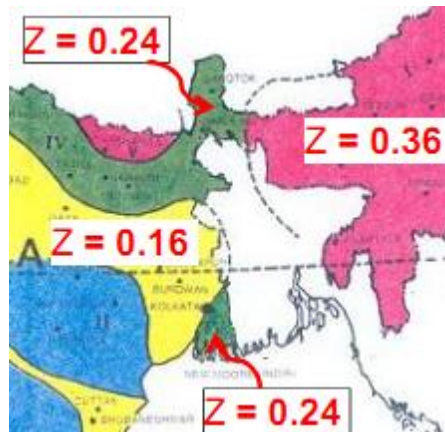

Figure 9: Seismic Zoning Map of neighbouring India based on Maximum Considered Earthquake (MCE).

Fig. 9 shows the seismic zone coefficients (MCE) for neighbouring India which has zone coefficients equal to 0.36, 0.24 and 0.16. Comparison between Fig. 8 and Fig. 9 shows that the Indian seismic zoning map has some agreement across the border with proposed seismic zoning map, however there are some differences in central-eastern (0.12 vs. 0.16, 0.2 vs 0.24) and south-eastern (0.28 vs 0.36) parts of Bangladesh. The higher values in Indian territory to the west of

Comilla and Chittagong can be accounted to the higher seismicity and closer proximity to the Indian-Burmese plate boundary fault systems.

On the other hand, comparing NDMA (2010) results (Fig.6) with the proposed zoning map (Fig.8), the PGA in Dhaka is 0.15g vs. 0.20g, in Chittagong 0.20g vs. 0.28g, in Sylhet 0.32g vs 0.36g. In other words, NDMA results are lower, more so in Dhaka and Chittagong.

In the updated BNBC, the design basis earthquake (DBE) ground motion is taken as 2/3 of the maximum considered earthquake (MCE) ground motion. Comparing with BNBC-1993, for some cities such as Chittagong, Faridpur, Rangpur, Pabna, Tangail, there is increase in design ground motion in the updated BNBC.

5 NEO-DETERMINISTIC SEISMIC HAZARD ASSESSMENT (NDSHA)

Neo-deterministic seismic hazard assessment (NDSHA) involves advanced numerical techniques to solve the wave propagation problem using properties of local geological structure and fault models. Synthetic seismograms are constructed by the modal summation technique using information on the source position and focal mechanism, maximum observed magnitude and wave propagation in anelastic media. This technique has been used to produce deterministic seismic hazard maps for different areas of the world (Panza et al., 1996; Parvez et al., 2003). The input data set consists of structural models, seismic source zones, focal mechanisms, earthquake magnitude and location. NDSHA has the advantage that it does not depend on empirical attenuation laws which are over-simplified. NDSHA studies for Bangladesh have been conducted in collaboration with University of Trieste, Italy with updated structural models. The seismic hazard expressed in terms of design ground acceleration (DGA) is extracted from the synthetic seismograms and mapped over the region of the study.
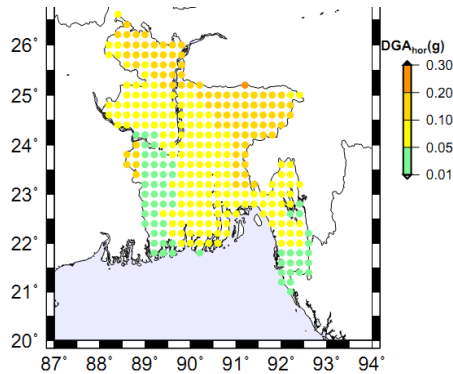

Fig.10 Estimated design ground acceleration (g) using NDSHA for a repeat scenario of 1897 M=8.1 Great Indian Earthquake
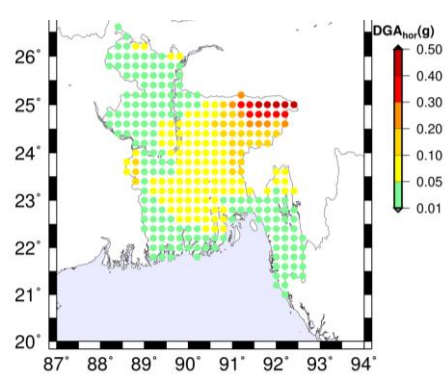
Fig.11 Estimated design ground acceleration (g) using NDSHA for a scenario M=8.0 Earthquake along Dauki Fault

NDSHA studies have been carried out to predict design ground motion for the case of repeat of some historical earthquakes or probable scenario earthquakes in Bangladesh. Fig. 10 presents computed design ground acceleration (g) in Bangladesh for repeat of M=8.1 Great Indian Earthquake at focal depth of 35 km. The strongest ground motion (0.1 to 0.2g) is in the bordering districts of Sylhet, Sunamganj, Netrokona, Mymensingh, Sherpur, Rangpur, Lalmonirhat, Lalmonirhat. These results appear to be within the design PGA values (DBE=2/3rd of MCE) of proposed zoning map of the Building code. However, if the magnitude is greater by +0.05, say M=8.1+0.5=8.6, then the ground motion will exceed the code provisions significantly in bordering districts. Fig.11 presents computed design ground acceleration (g) in Bangladesh for a scenario M=8.0 earthquake occurring at the Dauki fault along Sylhet-Mymensingh border at focal depth of 35 km. The strongest ground motion (0.3 to 0.5g) is in the bordering region of Sylhet, Sunamganj and Netrokona, which exceeds the code provisions.
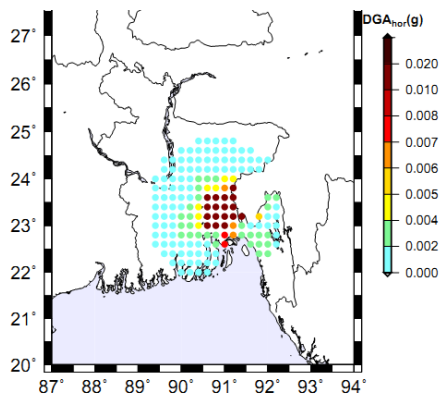

Fig.12 Estimated design ground acceleration (g) using NDSHA for a real M=5.1 Matlab Earthquake
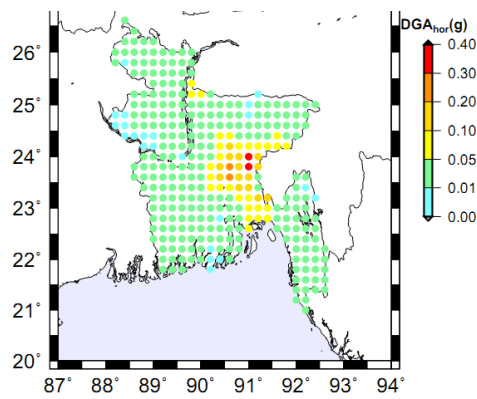
Fig.13 Estimated design ground acceleration (g) using NDSHA for a scenario M=7.0 Earthquake 50 km north of Matlab.

Fig. 12 presents computed design ground acceleration (g) in Bangladesh for a real M=5.1 Matlab Earthquake at focal depth of 18.4 km. Results show design ground acceleration of 0.002 to 0.004g in Dhaka city. Earthquake record in Dhaka city (courtesy of GSB) shows PGA value of 0.0066g. If we consider 2/3rd of PGA it comes to around 0.0044g. Next a scenario M=7.0 earthquake is considered. Its location is assumed to be 50 km north of the Matlab earthquake with a similar focal mechanism. This is considered in line with projected fault line system (Fig. 14) that is being considered by the Lamont Doherty Earth Observatory (LDEO), Columbia University scientists working in collaboration with Depart-

ment of Geology, Dhaka University under PIRE project. Through personal communication with them I have been informed that 7.0 or greater magnitude may occur along this extended fault system. The design ground acceleration is around 0.1g in Dhaka but it is 0.1g-0.3g around Comilla, thus exceeding DBE (2/3rd of MCE) motion of the proposed seismic zoning map.
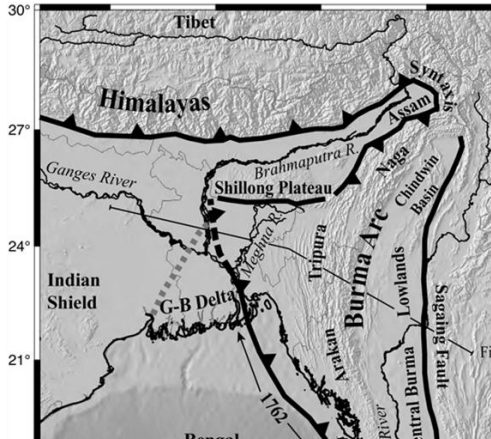

Fig.14 Projected fault (dashed line) extended north of Matlab, courtesy of PIRE project headed by LDEO (http://www.banglapire.org).
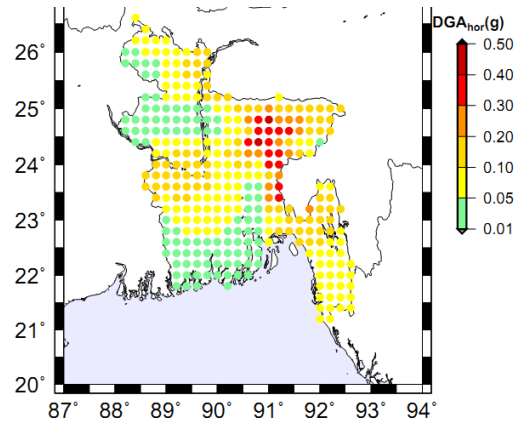
Fig.15 Estimated design ground acceleration (g) using NDSHA for a repeat scenario of 1918 M=7.6 Srimangal Earthquake

Fig. 15 presents computed design ground acceleration (g) in Bangladesh for repeat of M=7.6 Srimangal Earthquake at focal depth of 15 km. The strongest ground motion (0.2 to 0.4g) is in the neighbouring region of Sunamganj, Habiganj, Kishoreganj, Brahmanbaria which may exceed design PGA values (DBE=2/3rd of MCE) of proposed zoning map of the Building code.

6 CONCLUSIONS

This paper gives a brief account of several local as well as global and regional seismic hazard assessment studies that have included Bangladesh. As part of revising seismic design provisions of the Bangladesh building code (BNBC), PSHA studies have been conducted for Bangladesh. The concept of Maximum Considered Earthquake (MCE) motion having a 2475 years return period has been introduced. A new seismic zoning map has been proposed for the revised BNBC now awaiting publication. The country has been divided into four (instead of three) seismic zones with zone coefficient (Z) values of 0.12, 0.20, 0.28 and 0.36. The design basis earthquake (DBE) motion is taken as 2/3 of MCE motion.

The seismic zone coefficients are in reasonable agreement with those in neighbouring India except for central-western, central-eastern and south-eastern part. Compared to BNBC-1993, the design ground motion has significantly increased for some cities like Chittagong, Faridpur, Pabna, Tangail and Rangpur. Preliminary NDSHA studies have been conducted in collaboration with University of Trieste. Observing NDSHA results for two historical earthquakes, ground motion values may in some cases exceed proposed design acceleration values. Further refinement in NDSHA studies will be conducted as part of the ongoing study. NDSHA studies reveal that a probable scenario M=8.0 earthquake in Dauki fault or probable M=7.0 earthquake near Comilla can result in ground motion exceeding zoning map values in area around epicenter. These are earthquakes on locations suggested by recent seismological studies and lacking historical record. Implications of such findings by new seismological studies can therefore have great bearing on the probable ground motions. These new seismological discoveries should be well documented and gone through critical evaluation and validation before final acceptance.

ACKNOWLEDGEMENTS

REFERENCES

[1] Ali, M.H. and Choudhury, J.R. (1994) "*Seismic Zoning of Bangladesh*" paper presented at International Seminar on Recent Developments in Earthquake Disaster Mitigation, Dhaka, organized by Institution of Engineers, Bangladesh and World Seismic Safety Initiative (WSSI).

[2] Abrahamson, N. A. and Silva, W. J. (1997). "*Empirical Response Spectral Attenuation Relations for Shallow Crustal Earthquakes*", Seismological Research Letters, 68(1), 94-127.

[3] ADPC (2009) "*Risk Assessment of Dhaka, Chittagong and Sylhet City Corporation Area*" Main Report submitted by Asian Disaster Preparedness Centre for Comprehensive Disaster Management Programme (CDMP), Ministry of Food and Disaster Management, Government of of Bangladesh.

[4] Al-Hussaini, T.M. (2005) "*Facing the earthquake and tsunami risk in Bangladesh*" Proc., Seminar on Tsunami and Seismic Risk – Action for Bangla-

desh, organized by Military Institute of Science and Technology, Dhaka, 31-43.

[5] Al-Hussaini, T.M. and Al-Noman, M.N. (2010) "Probabilistic Estimates of PGA and Spectral Acceleration in Bangladesh", Proc. 3rd International Earthquake Symposium, Bangladesh, Dhaka, 473-480.

[6] Al-Hussaini, T.M. and Hasan, M.R. (2006). "Zonal Seismicity Characteristics in and around Bangladesh", Proc. 8th US National Conference on Earthquake Engineering, San Francisco, USA, paper no. 1945.

[7] Al-Hussaini, T.M., Hossain, T.R. and Al Noman, M.N. (2012) *"Proposed Changes to the Geotechnical Earthquake Engineering Provisions of the Bangladesh National Building Code"*, Geotechnical Engineering Journal of the SEAGS & AGSSEA, Vol. 43, No.2, 1-7.

[8] Ambraseys, N. and Bilham. R (2003) "Re-evaluated intensities for the great Assam earthquake of 12 June 1897, Shillong, India", Bull. Seismol. Soc. of Amer., 93(2), 655-673.

[9] Ansary, M.A. and Sharfuddin (2002) "Proposal for a new seismic zoning map for Bangladesh", Journal of Civil Engineering Division, Institution of Engineers Bangladesh, 30(2), 77-89.

[10] BIS (2005) "National Building Code of India 2005, part 6: Structural Design- Section 1: Load, Forces and Effects", Bureau of Indian Standards, 2nd revision.

[11] Bolt, B.A. (1987) *"Site Specific Study of Seismic Intensity and Ground Motion Parameters for Proposed Jamuna River Bridge, Bangladesh"* Report prepared for Jamuna Bridge Project, Bangladesh.

[12] DDC (1993a) *"Bangladesh National Building Code 1993"* published by Development Design Consultants for Housing and Building Research Institute, Dhaka, Bangladesh.

[13] DDC (1993b) "Seismic Zoning and Earthquake Risk of Bangladesh", Supplement to Bangladesh National Building Code 1993, published by Development Design Consultants for Housing and Building Research Instititute, Dhaka, Bangladesh.

[14] ICA (2000) "International Building Code", published by International Code Council, USA.

[15] Hattori, S. (1979). "Seismic Risk Maps in the World (Maximum Acceleration and Maximum Particle Velocity) (II) – Balkan, Middle East, Southeast Asia, Central America, South America and Others", Bulletin of the International Institute of Seismology and Earthquake Engineering, Building Research Institute, Ministry of Construction, Tokyo, 17, 33-96.

[16] Islam, M.S., Huda, M.M., Al-Noman, M.N. and Al-Hussaini, T.M. (2010) "Attenuation of Earthquake Intensity in Bangladesh" Proc. 3rd International Earthquake Symposium Bangladesh (IBES-3), Dhaka, 481-488.

[17] Kundu (1992). Magnitude-Frequency Relationship of Earthquake Occurrence in Bangladesh, M.Sc. Engg. Thesis, Bangladesh University of Engineering and Technology, Dhaka.

[18] Noor, M. A., Yasin, M. & Ansary, M. A. (2005) "Seismic Hazard Analysis of Bangladesh", Proc. 1st Bangladesh Earthquake Symposium, Dhaka.

[19] Panza, G.F., Vaccari, F., Costa, G., Suhadolc, P. and Faeh, D. (1996). "*Seismic Input Modelling for Zoning and Microzoning*", Earthquake Spectra, 12, 529-566.

[20] Parvez, I.A., Vaccari, F. and Panza, G.F. (2003). "*A Deterministic Seismic Hazard Map of India and Adjacent Areas*", Geophysics J. Int., 155, 489-508.

[21] UNAM (1999). CRISIS99 ver.1.017, Program for Computing Seismic Hazard, Revision 17 written by Ordaz, Aguilar & Arboleda, Instituto De Ingeneria, UNAM, Mexico.

REPAIR OF CRACKS ON THE DECK OF BANGABANDHU BRIDGE

Khan M. AMANAT[1], **A. F. M. S. Amin**[2], **M. Zakaria**[3] **and Jamilur R. Choudhury**[4]

[1, 2, 3] Professor, Department of Civil Engineering, Bangladesh University of Engineering and Technology, Dhaka, Bangladesh.
Email: [1]amanat@ce.buet.ac.bd

[4] Vice Chancellor, University of Asia Pacific, Dhaka, Bangladesh.
Email: jamilur.choudhury@gmail.com

Abstract. *Bangabandhu Bridge is a 4.8km long concrete box girder bridge built in 1998 on the Jamuna river. It is the only road and rail link between the north-west part and the other parts of Bangladesh. In 2006 and later, numerous longitudinal cracks were observed on the deck of the bridge. Investigation showed that there had been a design inadequacy which caused the development of these cracks. Repair of cracks started in 2011 and was finished in June 2013 at a cost of US$ 35 million (approx). The repair work had been a one-of-a-kind work manifesting an excellent example of modern engineering. The repair work involved use of CFRP strips glued to the deck surface in the transverse direction and covering it up with a mortar grout layer, water proofing membrane and stone mastic asphalt wearing course. An overview of the crack repair works carried out on the deck of the bridge, challenges faced and the measures adopted to mitigate the situations and issued occurred during the repair work etc. are described in this paper. The paper would enable the reader to have an in-sight into a most modern, technically challenging and one of the most extensive bridge repair work done recently.*

Keywords: Bangabandhu bridge, Box girder, Crack, CFRP, Repair, Strengthening, Epoxy, Testing.

1   INTRODUCTION

Bangabandhu Bridge, formerly known as Jamuna Multipurpose Bridge, or more colloquially Jamuna Bridge, is a 4.8km long concrete box girder bridge built in 1998 on the Jamuna River. The bridge, when constructed also stood as the 11th longest bridge in the world. The role of this bridge in the economy of Bangladesh is vital as it provides strategic economic road-rail-energy-telecommunication link between northern and southern part of the country, by crossing the Jamuna River, one of the widest river of the world. Superstructure of the bridge is of prestressed concrete box girder constructed using segmental construction technique. In 2006 and later, numerous longitudinal cracks were observed on the deck of the bridge. Investigation showed that there had been a design inadequacy which caused the development of cracks. Repair of cracks started in 2011 and was been finished in June 2013 at a cost of US$ 35 million (approx). The repair involved use of about 260,000m of CFRP strips, 3200m^3 of stone mastic asphalt and the service of more than 300 foreign workers over approximately two years time. The repair work has been a one-of-a-kind work manifesting an excellent example of modern engineering. An overview of the crack repair works carried out on the deck of the bridge, challenges faced and the measures adopted to mitigate the situations and issues occurred during the repair work etc. are briefly presented in this paper. The paper shall enable the reader to have an in-sight into a most modern, technically challenging and one of the most extensive bridge repair work done recently.

2   INVESTIGATION FOR THE CAUSES OF CRACKS

Bangabandhu Bridge has a history of cracks from the beginning of construction. Cracks appeared during construction at east approach viaduct, pier head units (first 13 units), deck slab surface, underneath of the soffit, hinge segment, segment adjacent to the hinge segment, pile cap shell and the pile stem. Most of these cracks were repaired by the contractor before commissioning of the bridge. However, few of these cracks, especially those on the deck of the bridge grew further and drew public attention in 2006. Bangladesh Bridge Authority (BBA) requested experts of the Department of Civil Engineering, Bangladesh University of Engineering and Technology (BUET) in March 2006 to conduct investigation to identify the possible causes of cracks.

Longitudinal cracks were observed at two distinct locations on the deck of the bridge. One were along the root of the south cantilever and other were along the middle of the box section (Fig.1 and 2). Though the railway track is located on the north side, no cracks were observed on that part of the deck.

In almost all the segments, longitudinal cracks were found clearly over the inside and outside faces of the south web. These cracks have formed primarily as shrinkage cracks as evidenced by the Bridge Consultants' (RPT-NEDCO-BCL) report where similar cracks were reported during erection of segments. These

shrinkage cracks opened further and became easily visible due to temperature variations.
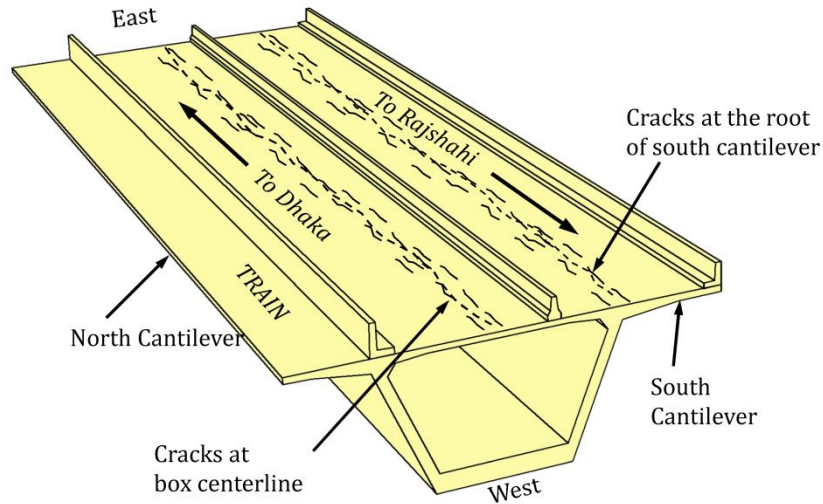

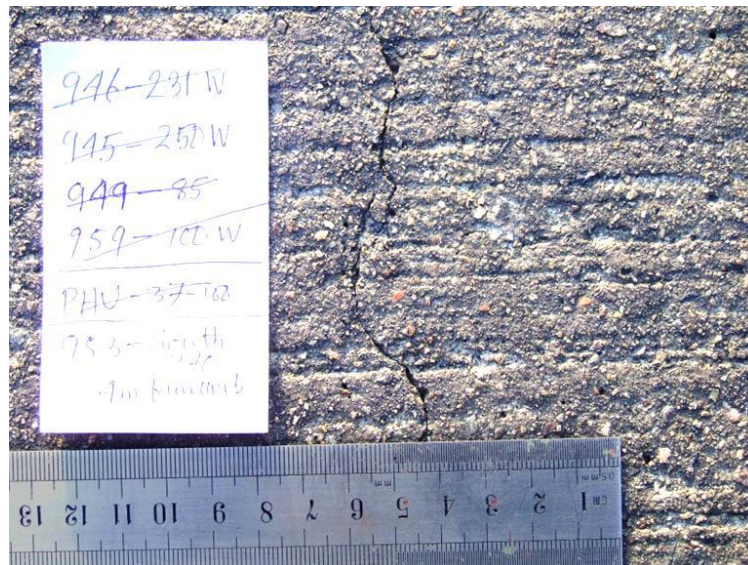Figure 1: Schematic representation of cracks on the deck of Bangabandhu Bridge

Figure 2: Typical example of a crack on the bridge deck

It is observed from the as built drawings that temperature and shrinkage steels provided in the top deck has been grossly inadequate with respect to the provisions of BS 5400: Part 4 which was referred to in the Jamuna Design Specifica-

tion (JDS) as Design Standard. These shrinkage and temperature cracks may have been significantly widened and more cracks became visible due to passage of heavily loaded trucks in the recent times over the bridge. It needs mentioning that 30 unit HB load along with appropriate HA loading combinations had been found to produce significant tension in the deck top adjacent to the inside face of the south web. So, it might be viewed as a design deficiency.

Distinct, more or less straight longitudinal cracks were observed in the top of the deck slab at center of the boxes. Similar cracks had been detected in some of the segments quite early during erection of the bridge segments. It is believed that these cracks have been initiated by shrinkage of concrete between two webs. Later they got widened due to temperature effects. Further, they got prominence due to negative temperature gradient (deck top colder than inside). BUET Consultants, from their 3-D analysis, obtained tension over 2.5 MPa on the top surface of box centre under self-weight and temperature gradient and the reinforcement provided for this at this location was inadequate.

3   REPAIR STRATEGY

After submission of the BUET report, Bangladesh Bridge Authority (BBA) appointed Filipino consulting firm Angel Lazaro and Associates (ALA) in 2008 to conduct a detailed investigation again and to suggest repair methodology. The findings of the investigation of ALA were similar to those of BUET report. In addition, ALA made a detailed design for the repair work. It has been pointed out that the cracks on the deck are in the longitudinal direction. This means, cracking stresses were developed in the transverse direction for which the transverse reinforcement was inadequate. Therefore any repair strategy should consider strengthening the deck in the transverse direction. BUET report also suggested "*Appropriate measures should be taken immediately to seal the cracks on the deck and lay 50 mm wearing course with material that can take significant tension and is abrasion-resistant.*" Regarding repair methodology, a number of repair techniques were available in literature. Considering the available techniques, ALA suggested that Carbon Fiber Reinforced Polymer (CFRP) strips may be glued on to the deck in the transverse direction to minimize further development of cracks. The CFRP strips shall be covered with a non-shrink mortar grout which shall be further overlaid by mastic asphalt concrete of 50mm thickness. A thermal insulation layer between the mortar grout and the asphalt layer was also suggested.

4   DESIGN ISSUES TO RESOLVE

Designing a sustainable repair strategy and implementing it on field both deserve equal attention and importance. As stated in the preceding paragraph, the proposed repair design involved use of CFRP, epoxy and other modern and synthetic materials. While short term mechanical performance of these materials is well

established and acceptable, their long term behavior under the stipulated conditions of use needed careful consideration.
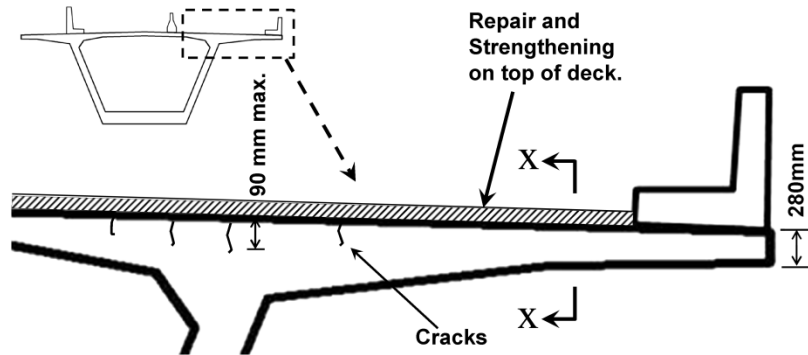

Figure 3: Repair and strengthening strategy on the deck

Epoxy is a universally accepted material in gluing the segment faces of box girder bridges. In most of such applications, the segment faces remain in compression and thus the use of epoxy does not pose and design difficulty. In the proposed repair methodology, epoxy was the principal material that would transfer the tension from deck to the CFRP strips. Therefore, performance of the epoxy adhesive had been of utmost important in this case. Since the repair would be on the top surface of the deck, it would be subjected to solar thermal radiation. If the glass transition temperature of the epoxy had been too low, natural solar heating in summer days might cause the temperature to easily reach or exceed the glass transition temperature and the epoxy would lose all its desirable mechanical and bonding properties leading to debonding of the CFRP and failure of the repair work. Therefore, the epoxy must have a high glass transition temperature, at least 20°C above the maximum possible deck temperature in summer.

Asphalt is kept quite hot when it is laid to facilitate roller compaction. Compared to normal asphalt, mastic asphalt generally has higher laying temperature. When such asphalt would be laid over the CFRP works, there would be possibility that the CFRP got damaged by the high temperature of asphalt. Therefore, the laying temperature of the asphalt must be kept as minimum as possible without compromising quality. Also the mortar grout must be capable of withstanding the heat of asphalt and should adequately shield the underlying CFRP from the heat.

The CFRP repair work including the mortar grout layer would be subjected to millions of cycles of direct bearing load from the wheels of vehicles over the years. Therefore, durability of the repair work under such adverse condition must also be ensured.

5   THE DESIGN FOR REPAIR AND STRENGTHENING

In 2011, Chinese company China Communications Construction Company (CCCC) was given the task of repairing the deck. After receiving the job, CCCC proposed some modification in the crack repair design. For example, they proposed stone mastic asphalt (SMA) instead of the conventional mastic asphalt. Also the laying temperature of the asphalt was revised. It was shown that the proposed revised design was a better choice and it was accepted. The final repair and strengthening scheme is described below.

The main strengthening element would be CFRP strips 100mm wide and 1.4mm thick. After cleaning the deck concrete using blast cleaner, these CFRP strips would be glued to the deck in the transverse direction for the full width of the vehicular carriageway using epoxy primer and epoxy adhesive. Spacing of these strips shall be 250mm on centers. After gluing the strips, a thin layer epoxy primer followed by non-shrink grout of thickness 10mm (6mm on CFRP) would be placed all over the carriageway to fully cover up the CFRP. Small stone particles would be scattered over the grout before hardening. These stone particles would facilitate mechanical interlocking with the stone mastic asphalt concrete layer to be placed later. Thereafter, a waterproofing membrane of thickness about 1.0mm would be sprayed on the grout. Finally, a 50mm thick layer of stone mastic asphalt shall be placed as a wearing surface. A schematic section (section x-x of Fig.3) of the adopted design of the repair work is shown in Fig. 4.
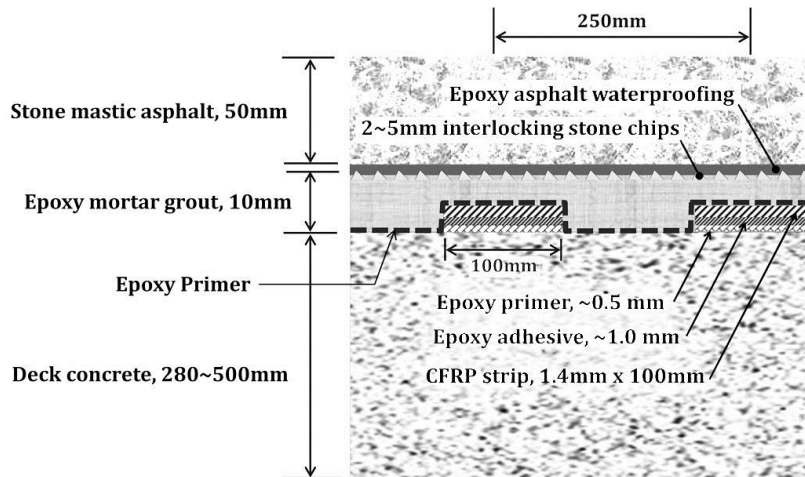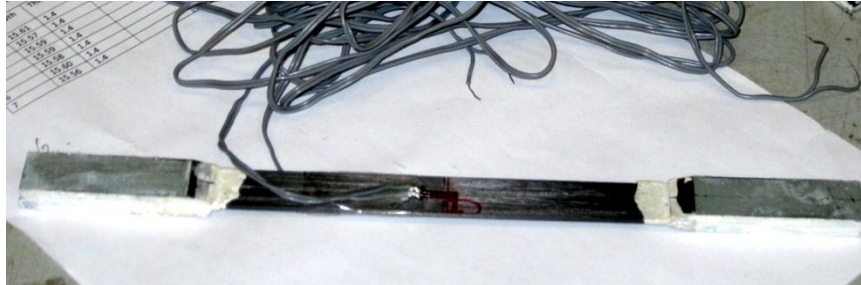

Figure 4: The deck strengthening design (Sec. x-x of Fig.3)

(a) CFRP tension sample fitted with strain gauge.

(b) Sample mounted in the testing machine.

(c) Sample after breaking.

Figure 5: Tension testing of the CFRP strips in NUS laboratory.

6   QUALITY ASSURANCE OF MATERIALS

Considering the nature, extent and uniqueness of the repair work, the importance of material testing by an independent laboratory of international standard to assure quality can never be overemphasized. The repair work involved many different specialized modern materials that included carbon fibre reinforced polymer (CFRP) strips, different types of epoxy primer, epoxy resins and epoxy adhesives etc.

For the CFRP strips, ensuring proper modulus of elasticity (about 200 GPa) and tensile strength (not less than 2800 MPa) was essential. Tensile strength test

(a) Tension and absorpsion samples of epoxy primer.
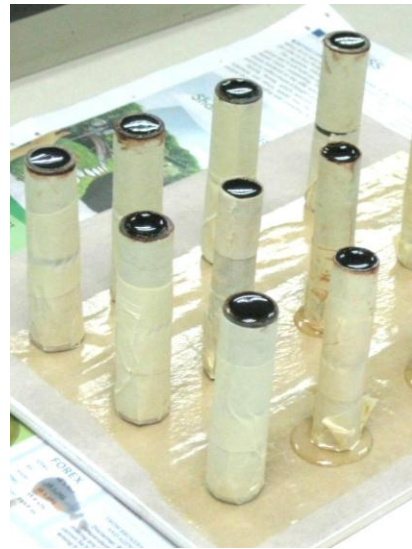
(b) Compression samples of epoxy primer.

(c) Epoxy bond test sample.

(d) Epoxy bond test sample after test.

Figure 6: Testing of epoxy materials at SETSCO Laboratory, Singapore.

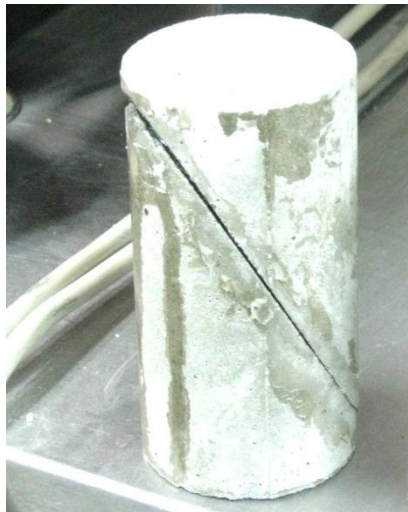(a) CCCC site office and laboratory.

(b) Testing machine in the site lab.

Figure 7: Site office and laboratory of the repair contractor.

(a)

(b)

Figure 8: Pictures of SMA batch mixing plant installed at site.

of CFRP was conducted in National University of Singapore (NUS). Some photographs of the tensile testing are shown in Fig. 5.

The epoxy materials were tested in the SETSCO laboratory of Singapore. Tests included a) compressive yield strength, Young's modulus, tensile strength and elongation at break at 14 days of aging, b) absorption (24 hours) at 14 days, c) viscosity, d) gel time, e) bond strength at 14days, f) linear coefficient of shrinkage on cure, g) sag flow, h) pot life etc. following appropriate ASTM, ISO and other standards as applicable. Some pictorial evidences of these tests conducted at SETSCO Laboratory are shown in Fig.6.

Besides testing of the materials in independent laboratories for their acceptance, an on-site laboratory was also established to continuously monitor the different required properties of all the materials. Fig.7 shows some photos of the on-site laboratory. It has been mentioned earlier that stone mastic asphalt (SMA)

was selected as the final wearing course material. To produce SMA with required properties, the contractor also installed a full-fledged batch mixing plant near the bridge site (Fig.8).

Figure 9: Debonded CFRP and mortar grout after a few days of 1st trial repair.

7 TRIAL REPAIR WORK

The finally approved design for repair and strengthening was selected through rigorous analysis and several reviews by experts. The quality of materials to be used in the repair works was also ensured through testing in independent laboratories abroad. Despite having confidence about the design and material quality, a provision for trial application was included in the repair contract. This was necessary because the nature and extent of the repair work itself was unique and the amount of monetary involvement was big. Therefore, before conducting the actual repair work, it was considered justified to verify the actual in-situ performance by implementing the proposed repair methodology on a section of the approach viaduct and subject it to regular traffic over a specified period of time. It was decided that, upon evaluating the performance of the trail repair work, necessary modification in the design shall be made if needed and further trial repair works shall be implemented. The actual repair work shall begin only after a fully satisfactory performance is achieved through trial repair works. The first trial repair work was conducted in March-April 2012 on the east approach viaduct slab of the bridge on a 70m long segment on the southern half of the carriage way. In the first stage, laying of epoxy primer, epoxy adhesive, CFRP strips and the mortar grout was done. The first glitch was encountered when it was found that debonding of CFRP from the deck occurred within a few days. It was observed that the CFRP strips along with the mortar grout could easily be peeled off within a few

days. It was observed that the CFRP strips along with the mortar grout could easily be peeled off from the deck by hand (Fig.9). Investigation by the experts and consultants revealed that strong ultra violet solar radiation prevalent at site caused the epoxy primer, which was kept bare open upon application, lose their bonding characteristics resulting in such failure. It was decided that to prevent such bond failure, the whole repair work should be kept covered with tarpaulin until laying of the SMA wearing course. Thereafter the trail repair work was implemented in full and was subjected to regular vehicular load. The season was the summer of 2012 and there had been some rain too. Thus the trial section was rigorously subjected to the most abusive condition that might occur in real life.

After about a few weeks, problems were encountered again. This time, it was observed that the mortar grout and the CFRP are getting separated from the deck along with a 12mm (approx.) layer of deck concrete with them. This time, failure of the deck concrete was causing separation of the whole upper layers. Occurrence of this failure of trial work raised serious concern among everyone involved in the project regarding the suitability of the suggested repair methodology. A renowned consulting firm AECOM from Hong Kong was employed by the contractor to investigate the matter and to provide a solution. According to their investigation, it was moisture or water ingression that caused such failure. Incompatible thermal expansion co-efficient of the mortar grout and the underlying deck concrete was also thought to be another principal reason behind this. The first trial work was implemented on the flat slab deck of eastern viaduct of the bridge which is spanning in the longitudinal direction between successive piers. The slab contained numerous cracks spanning in the transverse direction for the full width of carriage way. Some of these cracks were sealed from the bottom by the bridge contractor immediately after construction. However, the transverse cracks on the top surface near the piers were not treated. AECOM reasoned that water and moisture entered beneath the trial work through these cracks from the adjacent northern half of the carriageway and got entrapped beneath the trial work. Increase in ambient temperature as well as repetitive vehicular load caused this moisture to exert pressure on the concrete to failure. It was also pointed out by the experts that the thermal expansion co-efficient of the mortar grout was higher than that of concrete. Thus incompatible thermal expansion-contraction could be another reason behind this failure of the repair work. Following such suggestion, the mix ratio of the mortar grout was revised. AECOM suggested that, proper and durable water proofing of the deck must be ensured for the repair work to be a success. They also commented that the problem of water ingression would be less severe on the deck of the box girders because the cracks there are in the longitudinal direction which would be sealed by epoxy before application of the CFRP strengthening and also, unlike the first trial repair work, the actual repair would be carried out for the full width of the carriageway.

In order to ensure that the suggested mitigating measures would actually work, it was decided that a second trial repair work would be carried out – this time on the deck of the box girder. The second trial repair began in August 2012. Two lanes on the north side of the bridge about a 70m long section were blocked from traffic movement and the CFRP strips were attached. It was an Eid-Ul-Fitr vacation season and traffic volume was much higher than normal for carrying the vacationing people. Managing two way traffic with only two southern lanes was not adequate which resulted in a long traffic jam at the bridge site causing inconvenience to travelling people. To ease the situation, government ordered to open up the two blocked lanes before the second trial repair was completed. Heavily loaded trucks and buses were allowed to roll over the bare CFRP strips for about a week before these two lanes were blocked again. During this time, the CFRP strips were subjected to direct pressure and abrasion from the loaded vehicle wheels. A thorough inspection was carried out the assess damage done to the bare CFRP strips. Meanwhile, the contractor was able to fully prepare another trial segment of the bridge while the assessment of damage of the 2nd and incomplete trial repair was going on. To the relief of everyone, it was observed that no significant damage was done to the CFRP strips of the 2nd trial repair. It was thus proven that the CFRP and the adopted gluing system were quite robust. The third trial section was again subjected to vehicular traffic for several days. This time no distress or failure was observed. The third trial was proved to be a success. It was, thereafter, agreed that the actual repair work could be started following the revised design.

8   REPAIR OF THE BRIDGE DECK

To carry out repair of the deck, the bridge was divided into several segments along its length and the repair work progressed segment by segment. Length of each segment was about 700m. Of the 4 lanes, two lanes on one side of the median were repaired at a time while the other two lanes served the traffic, one in each direction. Over ten thousand vehicles pass over the bridge every day. Thus, traffic management on the bridge during the repair work was a big issue. For every segment the repair was done in several steps which are briefly described in the following paragraphs.

8.1 Initial Preparations and Cleaning

The actual repair work began with the removal of the median barriers. Thereafter, the deck concrete surface was cleaned using a blast cleaner. The blast cleaner (Fig. 10) used steel shots of approximately 1 mm diameter, which resembled mustard seeds, to clean the surface off the dirt, grease, etc.

(a) The blast cleaner machine

(b) Steel shots used in blast cleaning

Figure 10: The blast cleaner and the steel shots used

(a) Groove cutting along the cracks

(b) Filling the grooves with epoxy.

Figure 11: Groove cutting and filling of the cracks with epoxy.

(a) Strips of epoxy primer applied.

(b) Close-up view of epoxy primer strips.

Figure 12: Application of epoxy primer on the deck.

8.2 Crack Sealing

After cleaning the top surface, the next step was to seal the cracks. The initial proposition was that cracks wider than 0.2 mm shall be sealed by injecting low viscosity epoxy under high pressure. However, such attempts were failed several times and the process was abandoned. Instead, it was decided that 5mm wide and 5mm deep groves would be cut along the cracks using a concrete disk cutter and then the grooves would be filled with epoxy by gravity flow method. Typical pictures of grooves cut on the deck and later filled with epoxy are shown in Fig. 11.

8.3 Application of Epoxy Primer

The next step was to apply the epoxy primer on the cleaned surface of the deck in 100 wide strips, 250mm on centers. In order that the primer be fully effective in bonding with the concrete and the epoxy adhesive to be applied over it later, control of moisture and solar radiation was important. The surface moisture of the concrete must be less than six percent (6%) for the primer to be fully effective. After application, the deck was covered with tarpaulin to prevent solar UV radiation reach the primer. It was also ensured from the manufacturer that the glass transition temperature of the primer (as well as other epoxy materials) be at least $20^{o}C$ above the maximum possible temperature that would occur on the deck during the summer season. Typical photos of the application of epoxy primer on the deck are shown in Fig.12.

8.4 Laying the CFRP strips

Once the epoxy primer was cured adequately, the process of attaching the CFRP strips began. The process involved mixing together the two part epoxy adhesive in appropriate proportions, applying the adhesive over the primer using a template and a sliding hand mould so that a 100 mm wide and about 2mm thick layer of glue is placed uniformly, placing the CFRP strip on the epoxy adhesive and firmly attaching it to the adhesive using a hand roller, then putting RC blocks on the CFRP to ensure some pressure on the CFRP so that proper bonding occurs between CFRP and epoxy glue. The whole process was done manually strip by strip. Some typical pictures of the placing of CFRP strips are shown in Fig. 13.

8.5 Covering the CFRP Strips with Non-Shrink Mortar Grout

After the attachment of CFRP on the bridge deck, epoxy primer was applied all over again which was followed by application of non-shrink mortar grout to cover up the whole repair area. The thickness of the mortar grout was about 6mm over the CFRP strips and 10mm over the bridge deck concrete. Immediately after application of the mortar grout, small stone chips were scattered all over the top

surface of the mortar grout to facilitate bonding with the stone mastic asphalt layer to be applied later. Fig. 14 demonstrates a typical application of the mortar grout layer applied over the CFRP strips

(a) Putting epoxy glue in the sliding hand mould.

(b) Laying epoxy over primer by sliding the mould.

(c) A CFRP strip is being taken to place.

(d) CFRP strip placed on the epoxy glue.

(e) CFRP strips laid across the carriageway.

Figure 13: Different steps of application of CFRP strips.

(a) Mortar grout applied during 1st trial repair work.

(b) Mortar grout overlaid by scattered stone chips in actual repair.

Figure 14: Non-shrink mortar grout applied to cover up the CFRP strips.

(a) Epoxy asphalt water proofing membrane applied on mortar grout.

(b) Paving the carriageway with 50mm thick SMA.

Figure 15: Application of water proofing membrane and laying of the wearing course.

8.6 Applying Water Proofing Membrane and Laying of Asphalt

The last step of the repair work was to apply a 1mm thick water proofing membrane and to lay 50mm thick stone mastic asphalt (SMA) wearing course. The water proofing membrane comprised of epoxy and asphalt. Automatic paver machine was employed to lay the SMA. Fig.15 shows some photos of the water proofing membrane applied on the mortar grout and laying of the SMA.

(a) Dolly subjected to pull-off force by hydraulic jack.

(b) Pulled off dolly showing failure in concrete.

Figure 16: In-situ pull-off test on repair work.

9 IN-SITU TESTING

In addition to frequent laboratory testing of CFRP, epoxy and other materials during the repair work, in-situ pull-off tests of various components of the repair work was carried out to monitor the performance of the materials. Such testing is essential in maintaining the quality of the repair work. Pull-off strength of the epoxy adhesive and CFRP were the most important of these tests. To check the bonding strength of repair work with the concrete deck, a metal dolly was glued to the surface of the mortar grout using the epoxy. After adequate curing of the epoxy, circular peripheral groove was cut around the dolly down to the concrete deck. Then the dolly was subjected to pull-off load using a hydraulic jack until complete pull-off of the dolly occurred. Fig. 16 shows typical pictures of the dolly pull-off test of epoxy adhesive. It can be observed from Fig.16 that the pull-off failure took place in the concrete indicating that the bond behavior of the repair work is satisfactory. Similar pull-off test was carried out at every step of repair work to monitor the performance.

10 EPILOGUE

Considering the nature, extent, issues addressed and problems faced during implementation, the repair work on the deck of the Bangabandhu Bridge is undoubtedly a one-of-a-kind job that manifests a fine application of modern materials and engineering. The lessons learned and the experiences gathered from this project shall remain as an invaluable resource for the engineering community for years to come.

CYCLIC TESTS ON DIFFERENT SCHEMES OF RETROFITTING OF REINFORCED CONCRETE BEAM-COLUMN INTERIOR JOINTS

Raquib AHSAN

Department of Civil Engineering, Bangladesh University of Engineering and Technology, Dhaka, Bangladesh
Email: raquibahsan@ce.buet.ac.bd

Abstract. *This paper presents brief descriptions of cyclic tests on reinforced concrete (RC) beam-column interior joints that have recently been conducted at BUET. Non-seismic detailing of joints has been very common in Bangladesh and is a major cause of vulnerability of concrete frames built according to traditional RC construction practices. Cyclic behaviour of such joints has been investigated and compared to performance of seismically detailed joints. The specimen with non-seismic stirrup detailing and without ties at the interior joint region performed poorly. The reinforced concrete beam-column interior joints with seismic ties at the joint region showed improved performance with respect to absorbed energy, resisting moment and secant stiffness. Inadequate joints were retrofitted separately using tie bars, Carbon Fibre Reinforced Polymer (CFRP), Fibre Reinforced Concrete (FRC) and Ferrocement. Cyclic tests have been conducted on these joints. Joints strengthened by CFRP fabrics exhibited better ductility and strength than those of the joints retrofitted by CFRP plates or tie bars. Failure of all specimens retrofitted by FRC or ferrocement occurred away from the beam-column joints which conclude that any of these materials can be used satisfactorily as retrofitting materials for joints in seismic design.*

Keywords: Cyclic test, Retrofitting, Beam-column interior joint, CFRP, FRC, Ferrocement.

1 INTRODUCTION

Beam Column joints in reinforced concrete buildings experience large shear forces during seismic events and the joints without seismic detailing may undergo brittle failure. The joint failure is dominated by slip of the longitudinal reinforcement and joint shear deformation [1]. Researches have shown that poor design and detailing of joints may lead to a total or partial collapse of buildings [2-5]. Beam-column joints have a very important role on the overall ductility of the structure [3, 6]. Shear failure at the joints is brittle in nature and not desirable. Thus the non-seismically detailed joints should be strengthened to move the failure to the beams.

A large number of researches have been carried out on the cyclic behaviour of beam-column joints in last couple of decades. Many researchers conducted experiments on exterior joints [1, 5, 7-12]. Among them Akguzel and Pampanin [1], Sezen [5], Mahini and Ronagh [7], Sharma et al. [8], Pandelties et al. [9] and Ilki et al. [10] strengthened the joints by FRP composite materials. Tsonos [11] used concrete jacketing as a strengthening measure of exterior joints. Ravichandran & Jeyasehar [12] carried out an experimental investigation on post seismic retrofitting of exterior beam column joints using ferrocement.

Some researchers conducted experiments on unretrofitted interior joints [4, 6, 13]. Shiohara and Kusiara [4] investigated the effects of (i) amount of longitudinal reinforcement, (ii) column to beam flexural strength ratio and (iii) column to beam depth ratio on lateral capacity and post-yielding behaviour of interior joints. Pampanin et al. [6] reproduced structural inadequacies in joints, typical of the Italian construction practice in the mid '70s. An apparent satisfactory level of deformability as well as ductility, due to the combined effects of slippage phenomena and low column reinforcement ratio, were observed in interior cruciform subassemblies. The test results indicated that shear capacities of some specimen fall 5% to 30% short of the shear calculated from flexural strength of beam or column. Joh and Goto [13] observed that joint shear strength was increased by the existence of transverse beams in the interior joints.

Few researchers conducted research on the behavior of retrofitted RC interior beam-column joints [14-17]. Mukharjee and Joshi [14] used FRP plates to increase the shear and flexural strength of the beam. Almusallam and Al Salloum [15] demonstrated that externally bonded FRP sheets can effectively improve the shear strength and ductility of interior beam-column joints. Li and Qi [16] showed that repair of damaged RC beam-wide column interior joints by FRP can restore the performance of the damaged joints. Rai [17] tested damaged joints retrofitted with epoxy injection and carbon fibre wrap. These studies were conducted on interior joints which did not include transverse beams and slabs.

In the present study, performance of RC interior joints, with typical detail of traditional construction practice in Bangladesh, has been investigated in comparison with seismically detailed control sample. Physical models were prepared

with beams in both directions and floor slab in order to replicate the constructional difficulties of retrofitting interior joints. The interior joints were retrofitted in five ways: (i) by inserting CFRP plate into the beam-column joint, (ii) wrapping beam and columns by CFRP fabrics, (iii) with tie bars in the joint region, (iv) with polyester fibre-reinforced concrete and (v) with ferrocement. Cyclic behaviour of each retrofitting scheme is investigated and compared with each other.

2   INTERIOR JOINTS WITHOUT TIES IN THE JOINT REGION

Seven half-scale specimens of reinforced concrete beam-column joints were constructed considering two parameters. These test parameters were a) joint region with and without seismic ties and b) different column to beam cross-section ratios. Details of the specimens are shown in Figures 1 to 3. 30 MPa stone chips concrete and 500 MPa steel was used to prepare the specimens.
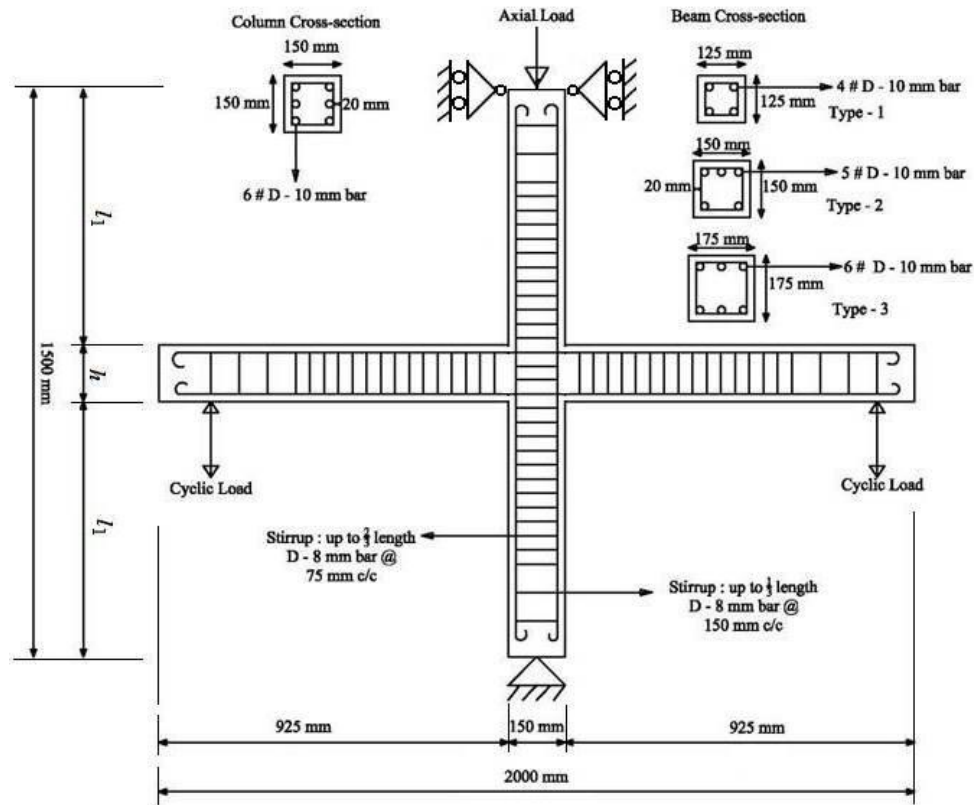

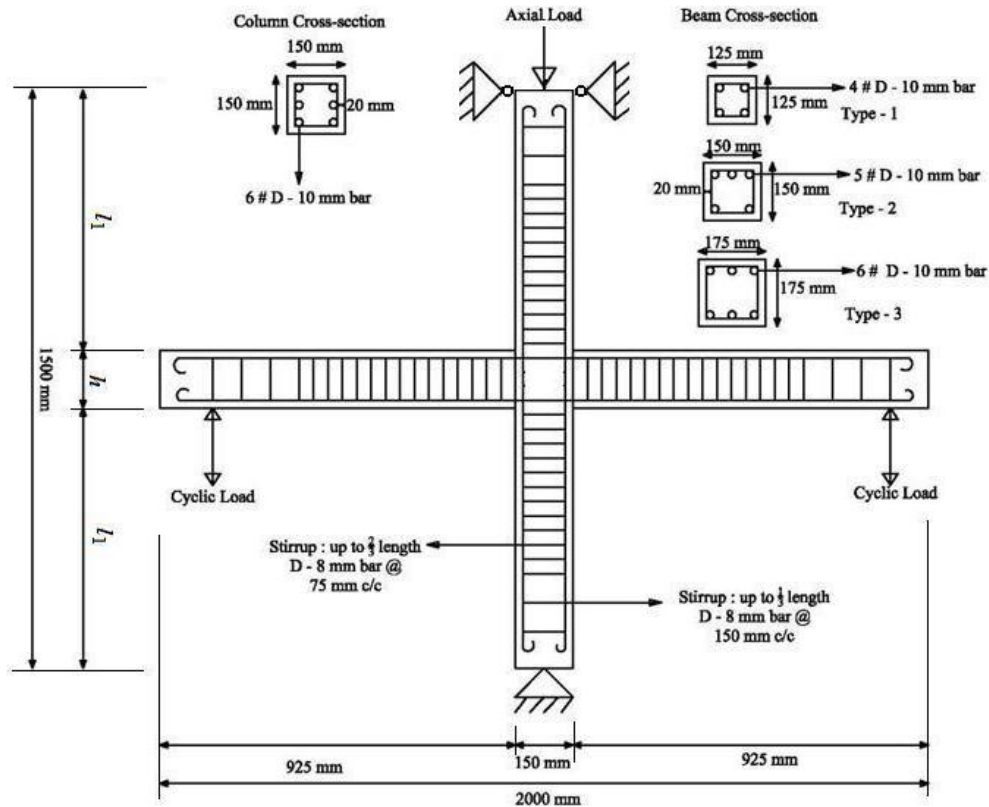Figure 1: Beam-column joints with ties at joints (Type – 1A, 2A, 3A).

Figure 2: Beam-column joints without ties at joints (Type – 1B, 2B, 3B).

The specimens were subjected to cyclic incremental moment with sustained gravity load. The experimental setup is shown in Figure 4. The beam-column joints were tested under vertical incremental cyclic loading at the ends of the beam along with constant axial load on the column. Vertical loading was applied at the end of beam using displacement control. A constant loading rate per cycle was maintained until the specimens experienced significant loss of capacity. The loading history applied to the specimens is shown in Figure 5.

Sample cracking patterns of specimens 2A, 2B and 2C are shown in Figures 6(a) to 6(c). Moment-rotation response of specimens 2A, 2B and 2C are shown in Figures 7(a) to 7(c). Skeleton curves of moment-rotation relationship of the seven samples are compared in Figure 8.

Beam-column joints with seismic ties exhibited better seismic performance than the joints without ties. Beam-column joints without ties showed diagonal cracking at maximum load of fourth cycle where joints with ties expressed vertical cracking at the faces of the joint where the beams frame into the joint. Beam-column joints without ties in the experiment were almost 15% - 20% less strong
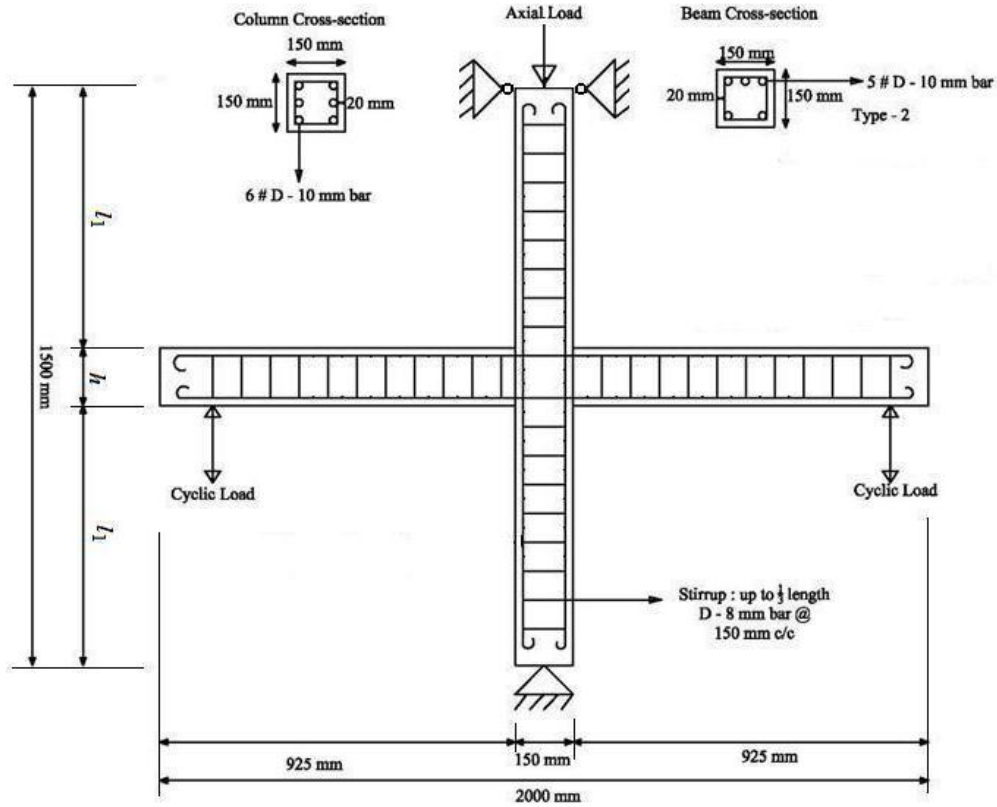
than beam-column joints with ties.

Figure 3: Conventional beam-column joint of without ties at joint (Type – 2C).

3 INTERIOR JOINTS RETROFITTED WITH FRP

This experimental study is under taken to study the behavior of RC interior beam-column joints which lack in shear reinforcement and strengthened by FRPs and additional tie bars. The samples are constructed with transverse beams and slab. Total eight models have been prepared of which three joints have been strengthened by Carbon FRP (CFRP) Fabrics, two joints have been strengthened by CFRP Plates and one model has been strengthened by adding tie bar into the joint. The samples have been subjected to incremental cyclic loading provided by hydraulic jacks under constant axial or gravity load and their load-deformation behaviors have been measured by dial gauges and video extensome-ter. Behaviour of the strengthened joints is compared with that of the control model.
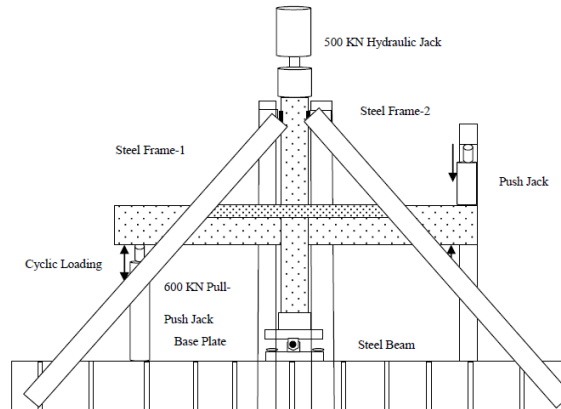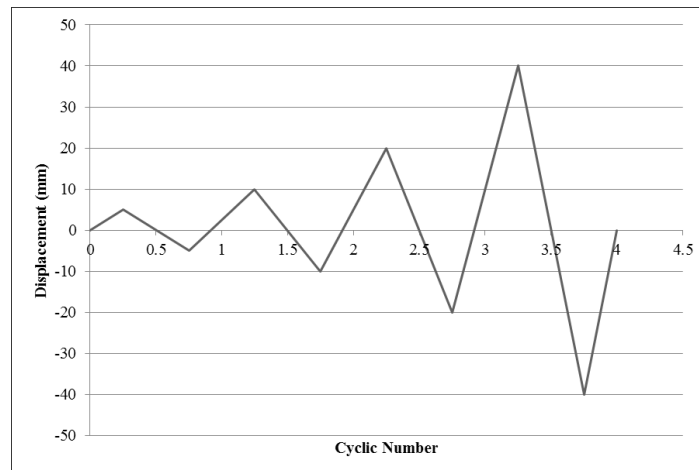
Figure 4: Experimental setup.

Figure 5: Applied displacement type of loading history.
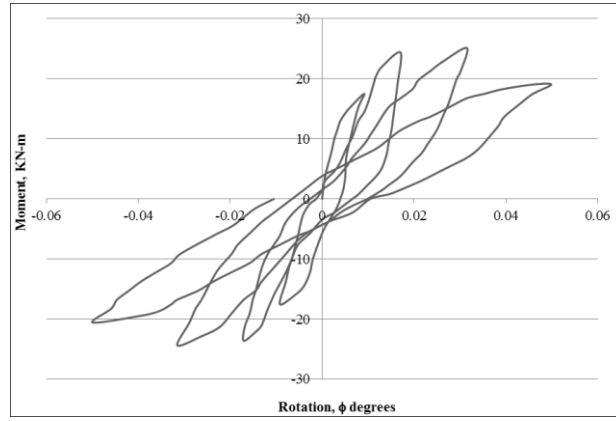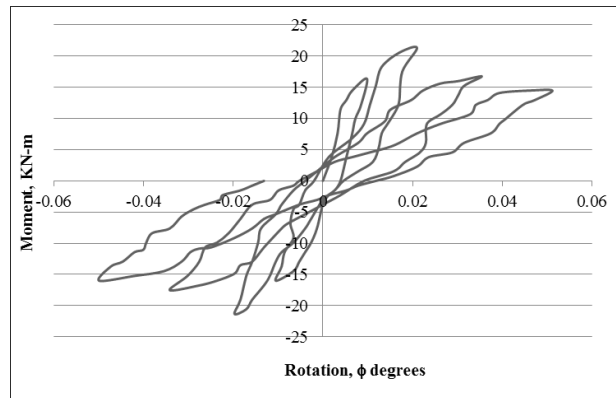

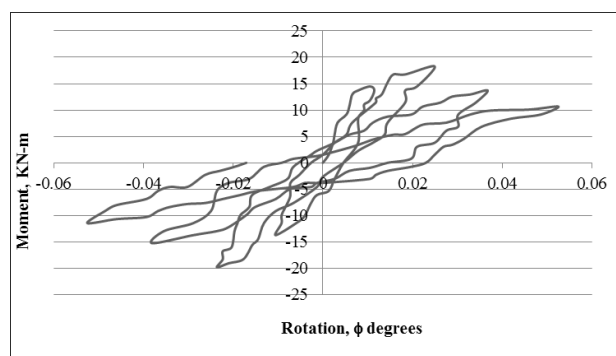(a) Sample 2A   (b) Sample 2B   (c) Sample 2C

Figure 6: Cracking pattern.

(a) Sample 2A

(b) Sample 2B
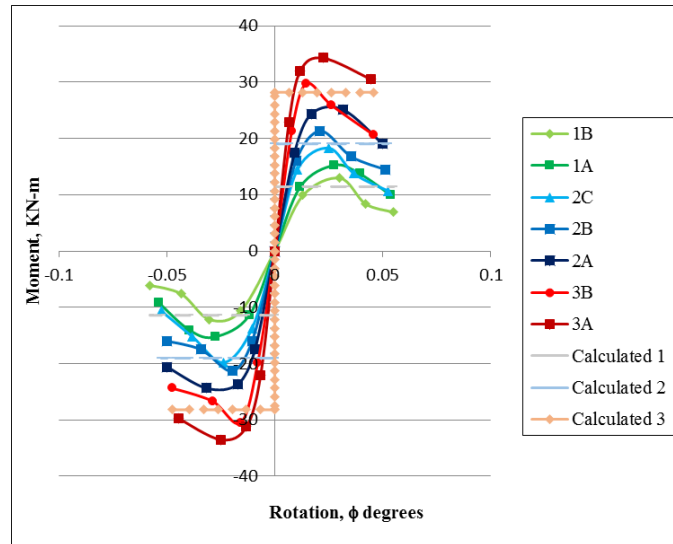

(c) Sample 2C
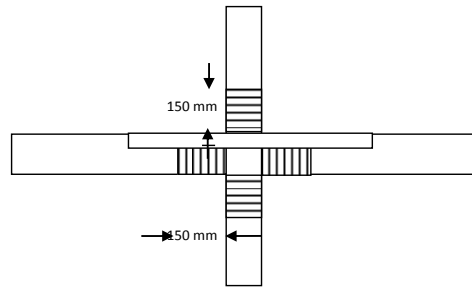
Figure 7: Moment-rotation response.

Figure 8: Skeleton curves of moment-rotation response of unretrofitted joints

27 MPa brick chips concrete and 500 MPa reinforcement was used to prepare the samples. Tensile strength of CFRP fabric was 4.9 GPa and that of CFRP plate was 2.8 GPa. Interior RC joints were retrofitted in three different schemes as shown in Figure 9. In the first scheme top and bottom Columns were wrapped up to 150 mm from the top of the slab and bottom of the deeper beams respectively as shown in Figure 9(a). Beams were wrapped up to 150 mm length in U shape from the face of the column.

In Second scheme, the joints were strengthened by introducing FRP plates into the joint. The concrete from beam at column face, up to a distance of 75 mm, were removed to insert the CFRP plates. CFRP plates were cut into pieces of 300 mm in length. Each of the joints was strengthened by four plates as shown in Figure 9(b).

In the third scheme, concrete up to 75 mm from the face of the beam was removed from all sides of the corner joint region. 8mm Φ tie bars each of 200 mm in length were welded around the column as shown in Figure 9(c).

Skeleton curves of moment-rotation relationships of different schemes are shown in Figure 10. The rotational capacity of the joints can be increased by strengthening the joints by CFRP Plates. Rotational stiffness of these joints was higher than that of the control model. Rotational stiffness of these joints also decreased gradually. From moment-rotation curves, it is found that BC joints strengthened by CFRP Plates show ductile behavior. CFRP Plate is effective in resisting diagonal crack travelling to transverse beams. It can be concluded that location of plastic hinge may be altered by altering the length of the plate.

(a) Scheme 1: Wrapping by CFRP fabric.
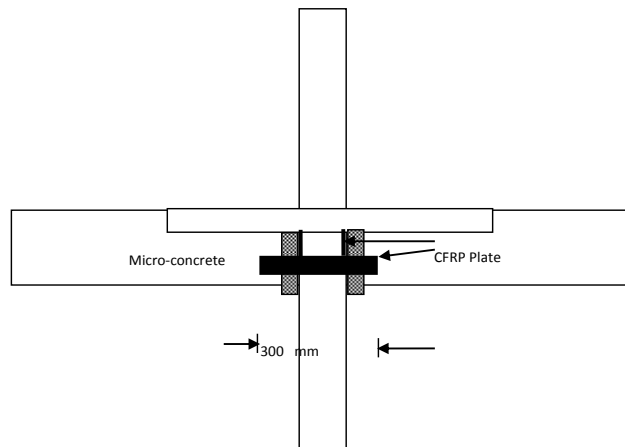
(b) Scheme 2: Inserting CFRP plates.
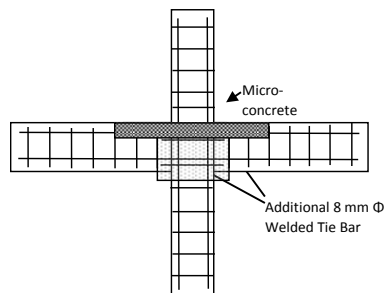
(c) Scheme 3: Welding tie bars.

Figure 9: Different schemes of retrofitting interior joint using CFRP or tie bars.

Figure 10: Skeleton curves of moment-rotation response of different schemes of retrofitting.

Joint retrofitted by micro-concrete and additional tie bar underwent large deformation before failure exhibiting ductile be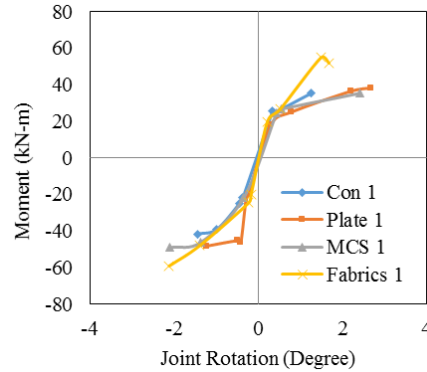havior of the joint. Moment capacities of the joints strengthened by CFRP Fabrics were higher against the same rotations compared to the control models. Joints strengthened by CFRP fabrics exhibited better ductile behavior than the control models. The mode of failure may be shifted from column to beam by strengthening joints by CFRP fabrics, since column shear and flexural capacity can be increased by CFRP wrapping.

4 INTERIOR JOINTS RETROFITTED WITH FERROCEMENT AND POLYSTER FIBRE REINFORCED CONCRETE

Seven half scale columns were constructed. Three of them were retrofitted by Ferrocement with varying volume fractions (0.99%, 1.62% and 2.43%) and another three of them were retrofitted by Fibre Reinforced Concrete (FRC) with varying dosages of polyester fibre (0.1%, 0.2% and 0.3% of concrete volume). The rest one was kept as control specimen. Then the specimens were tested under deflection control cyclic loading with a constant axial load. Their load-deformation behavior has been measured by dial gauges and video extensometer. Behavior of the strengthened joints is compared with that of the control specimens considering appearance of first crack, maximum load, deflection and failure patterns, rotation with respect to applied moment, stiffness and rotational stiffness.

20 MPa stone chips concrete and 500 MPa reinforcement was used to prepare the samples. 30MPa mortar was used for ferrocement. Recron 3s polyster fibre with tensile strength of 578 MPa was used for FRC. The mixing ratio and water-cement ratio were kept 1**:**2.18**:**3.7 and 0.48 respectively, by weight, to produce FRC. Admixture Glenium 30 was used as 0.4% of cement by weight to maintain the workability of the FRC. Tensile strength of concrete was found to increase

from 15% to 40% for varying ratios of fibre. A description of test specimens is given in Table 1. A photograph of the specimens is given in Figure 11. Steps of retrofitting with ferrocement are shown in Figure 12 and those of retrofitting with FRC are shown in Figure 13. Experimental setup is shown in Figure 14.

Sample moment-rotation behaviour of different types of joints are shown in Figure 15. Skeleton curves of moment-rotation response of Group A and Group B joints are shown in Figures 16(a) and 16(b) respectively.

Table 1: Description of test specimens.

Group	Specimen Designation	Retrofitting Methodologies
	Specimen-C	Control specimen
Group A	Specimen-F1	Ferrocement with wire mesh of 0.7 mm dia and 6.25 mm opening ($V_f = 0.99$)
	Specimen-F2	Ferrocement with wire mesh of 1.1 mm dia and 9.375 mm opening ($V_f = 1.62$)
	Specimen-F3	Ferrocement with wire mesh of 1.1 mm dia and 6.25 mm opening ($V_f = 2.43$)
Group B	Specimen-R1	Fibre Reinforced Concrete having 0.1% of Recron 3s
	Specimen-R2	Fibre Reinforced Concrete having 0.2% of Recron 3s
	Specimen-R3	Fibre Reinforced Concrete having 0.3% of Recron 3s

Figure 11: Interior beam-column joint specimen.

(a) Chiselling concrete surface

(b) Placing wire mesh

(c) Addition of cement mortar

(d) Curing
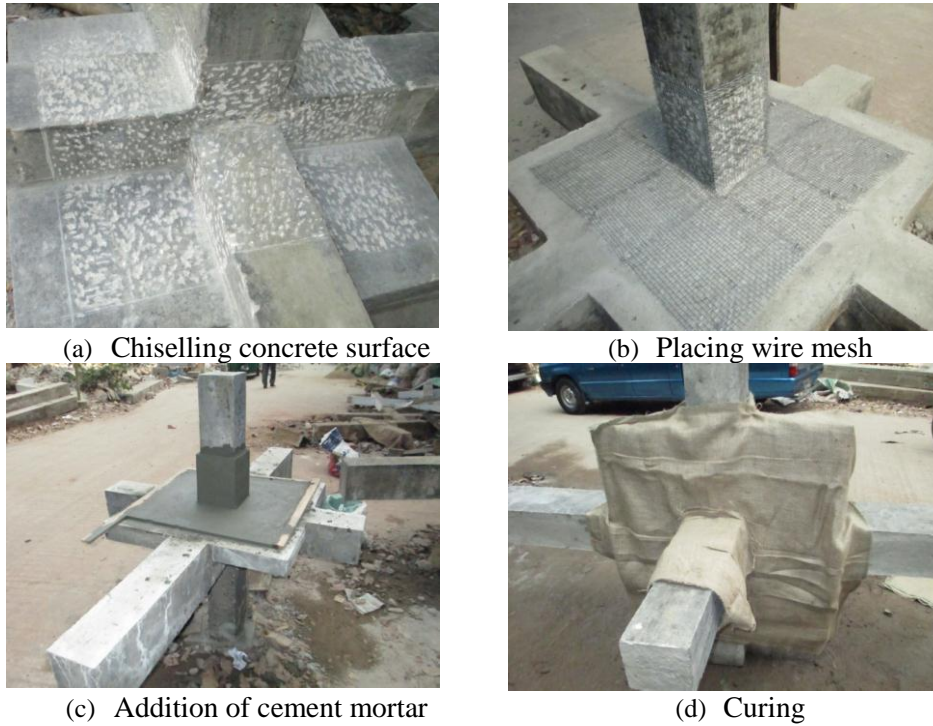
Figure 12: Steps of retrofitting with ferrocement.

(a) Chiselling and insertion of nails

(b) Placing of FRC
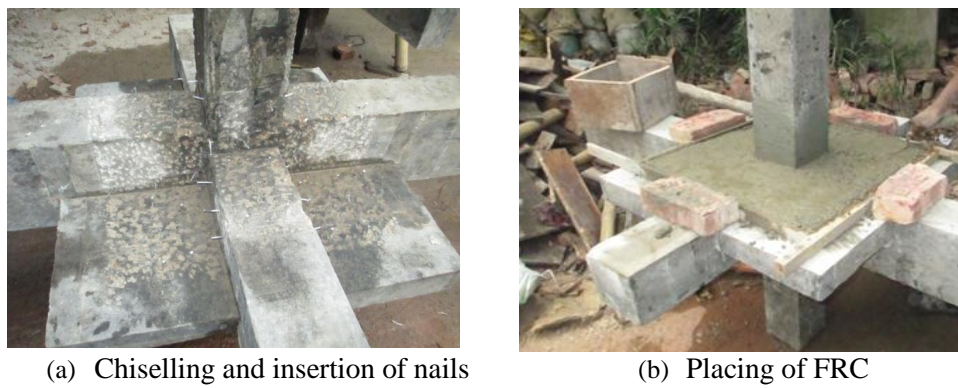
Figure 13: Steps of retrofitting with FRC.

Figure 14: Experimental setup.

(a) Control specimen (b) Sample F1 (c) Sample R1
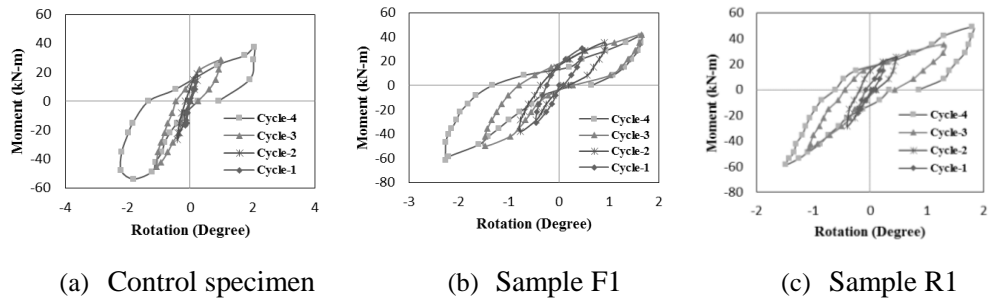
Figure 15: Sample moment-rotation behaviour of different types of joints.

(d) Group A (e) Group B
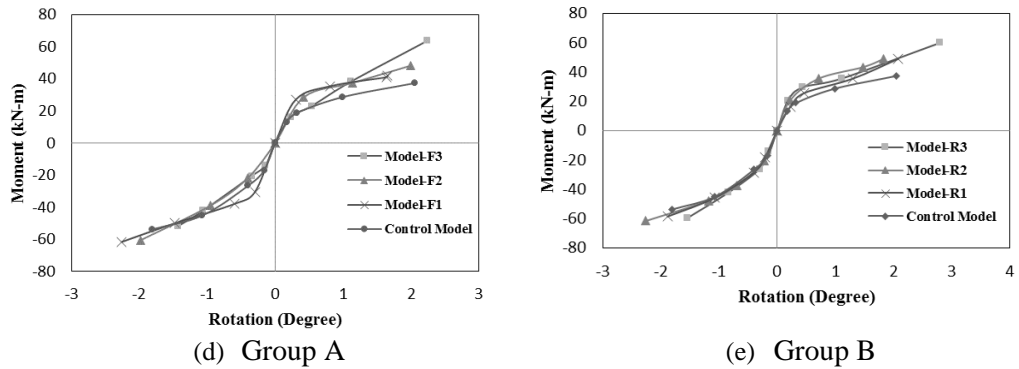
Figure 16: Skeleton curves of moment-rotation response.

It was found from the tests that ductility of joint can be increased by retrofitting the joint with ferrocement as well as FRC. Joint rotation was 51% more for Group A, and 69% more for Group B, than the control specimen before failure.. Rotational stiffness of the beam-column joints can also be improved by retrofit-

ting the joints. The initial rotational stiffness of column joint is increased up to 22% while retrofitting by ferrocement and up to 41% while retrofitting by FRC. Moment capacity of the joint is increased up to 15% by strengthening with both the ferrocement and FRC. Finally the failure of the control specimen occurred at the beam-column joint due to the lack of shear reinforcement at the joint. On the other hand the failure of the all retrofitted specimens occurred away from the beam-column joint which conclude that both the ferrocement and FRC can be used satisfactorily to retrofit the joints.

5   CONCLUSIONS

- Interior joints without ties at the joint region perform poorly compared to those with ties at the joint region.

- All five retrofitting schemes using CFRP fabric, CFRP plate, additional ties, ferrocement and FRC yield satisfactory performance of the interior joints.

- From the point of view of constructional ease, CFRP fabric, ferrocement or FRC may be more preferred compared to other methods.

- Ferrocement and FRC are more cost effective that other methods.

- In consideration of wide range availability of both material and skill necessary for ferrocement, retrofitting of interior joints with ferrocement has very good prospect in Bangladesh.

- Extensive experimental studies are required to develop design guideline for retrofitting of interior RC joints with available local materials.

REFERENCES

[1] U. Akguzel, S. Pampanin. 2012. Assessment and design procedure for the seismic retrofit of reinforced concrete beam-column joints using FRP

composite materials. *ASCE, Journal of Composites for Construction*, **16(1)**, pp 21-34.

[2] A. Prota, A. Nanni, M. Gaetano, E. Cosenza 2004. Selective upgrade of under designed reinforced concrete beam-column joints using carbon fiber reinforced polymers. *ACI Structural Journal*, **101 (5)**, pp 699-707.

[3] S.R. Uma, A.M. Prasad. 2005. Seismic behavior of beam column joints in reinforced concrete moment resisting frames. *Document no. IITK-GSDMA-EQ-31-V1-0, IITK-GSDMA Project on Building Code*.

[4] H. Shiohara, F. Kusiara. 2010. An overlooked failure mechanism of reinforced concrete beam-column joints, *Proceedings of the 9th U.S. National and 10th Canadian Conference on Earthquake Engineering*, Toronto, Ontario, Canada, July 25-29.

[5] H. Sezen. 2012. Repair and strengthening of reinforced concrete beam-column joints with fiber reinforced polymer composites. *Journal of Composites for Construction*, *ASCE*, **16(5)**, pp 499-506.

[6] S. Pampanin, G.M. Calvi, M. Moratti. 2002. Seismic behaviour of R.C. Beam-column joints designed for gravity loads. *12th European Conference on Earthquake Engineering*. London, UK. September.

[7] S.S. Mahini, H.R. Ronagh. 2007. A new method for improving ductility in existing RC ordinary moment resisting frames using FRPs. *Asian Journal of Civil Engineering (Building and Housing)*, **8(6)**, pp 581-595.

[8] A. Sharma, G. Gension, G.R. Reddy, R. Eligehousen, S. Pampanin, K.K. Vaze. 2010. Experimental investigations on seismic retrofitting of reinforced concrete beam-column joints. *14th Symposium on Earthquake Engineering*, Indian Institute of Technology, Roorkee, December 17-19.

[9] P.C. Pantelides, C. Clyde, L. Dreaveley. 2000. Rehabilitation of R/C building joints with FRP composites. *12 WCEE Conference*, Auckland, New Zealand., 30 January-04 February.

[10] A. Ilki, I. Bedirhangolu, N. Kumbasa. 2011. Behavior of FRP-retrofitted joints built with plain bars and low strength concrete. *Journal of Composite Construction, ASCE*, vol.15, No 3, pp 312-326.

[11] A.G. Tsonos. 2000. Lateral load response of strengthened reinforced concrete Beam-to-column joints, *12 WCEE Conference*, Auckland, New Zealanl9d, 30January-04 February.

[12] K. Ravichandran, C.A. Jeyasehar. 2012. Seismic retrofitting of exterior beam column joint using ferrocement, *International Journal of Engineering & Applied Sciences*, **4(2)**, pp 35-58.

[13] O. Joh, Y. Goto. 2000. Beam column joint behavior after beam yielding in R/C ductile frames. *12 WCEE Conference*, Auckland, New Zealand, 30January-04 February.

[14] A. Mukharjee, M. Joshi. 2005. FRPC reinforced concrete beam-column joints under cyclic excitation. *Journal of Composite Structure*, **70(2)**, pp 185-199.

[15] H.T. Almusallam, Y. Al Salloum. 2007. Seismic response of interior RC beam-column joints upgraded with FRP sheets. I: experimental study. *ASCE Journal of Composites For Construction*. **11(6)**, pp 575-589.

[16] B. Li, Q. Qi. 2011. Seismic behavior of the reinforced concrete interior beam-wide column joints repaired using FRP. *Journals of Composites for Construction*, *ASCE*, **15(3)**, pp 327-338.

[17] G.L. Rai. 2007. *Short-term and long-term performance of externally pre-stressed RC beams and joints, PhD Thesis*, Indian Institute of Technology Bombay.

EMPOWERING BIM THROUGH APPROPRIATE PROCUREMENT STRATEGY

M. Motiar RAHMAN

Institut Teknologi Brunei, Gadong, Brunei Darussalam
Email: motiar.rahman@itb.edu.bn

Abstract. *Compared to the static 2D or 3D drawings, Building Information Modelling (BIM) allows time sequencing (i.e. 4th Dimension) in visual environments in demonstrating the construction process, before any real construction activities take place, and throughout the whole lifecycle of the structure. Diverse advantages of BIM include selection of appropriate construction materials, identification of possible mistakes and conflicts at early project stages and prediction of the appropriate construction schedule and method. BIM can be furthered to nD modelling, e.g. by incorporating issues like cost (i.e. 5th dimension), sustainability and accessibility, to portray a holistic model and visually project the building design over whole project lifecycle. These are achieved by developing project specific multi-dimensional intelligent models. While advantages of BIM are well documented, its adoption is inhibited by multiple issues, e.g. legal and contractual issues, data copyright, mismatch of capabilities of different contract parties and interoperability of software. However, selecting an appropriate procurement strategy is probably more important for BIM adoption, since BIM process and procurement strategy are coupled together. This paper examines the suitability of the available procurement approaches, to support BIM and thereby to overcome those barriers, as well as to harvest enhanced benefits. It is observed that collaborative procurement arrangements provide suitable platform for BIM, and the more integrated the procurement arrangement is, the more suitably it contains and supports BIM.*

Keywords: BIM, Construction, Integration, Procurement, Teamwork.

1 INTRODUCTION

One of the major challenges the construction industries are facing today is how to improve efficiency. As such, literature abounds in suggesting integration of design and construction processes, as well as adoption of Building Information Modelling (BIM), for performance gains. This requires selecting an appropriate procurement strategy, to ensure the effectiveness of the integrated design and construction process, and also to accommodate BIM at the same time, where collaborative efforts of contract parties can develop effective design, execute efficient construction and practice smooth contract management. In this context, this paper first briefly introduces various aspects of BIM. It then presents an analysis of the available procurement strategies, for their suitability to contain BIM, and empower BIM adoption.

2 BUILDING INFORMATION MODELLING (BIM)

Traditionally, engineers used paper, pencil and ruler to visualize and describe buildings and designs in 2 dimensional (2D) planar states, i.e. X and Y axes. Depicting Z axis as height became much easier with the advent of AutoCAD, and the process of design changed and improved rapidly [1]. However, 3D modelling in construction goes beyond the object's geometric dimensions and replicates visual attributes such as color and texture. Time sequencing of such 3D geometric model in visual environments is commonly referred to as 4D modelling [2]. 4D modelling allows demonstration of the building construction process before any real construction activity takes place, helps to identify any possible mistakes and conflicts at early project stages, and enables prediction of construction methods and schedule [1]. nD modelling extends the concept of 4D modelling, and further integrates 'n' number of design dimensions, in a holistic model to portray and visually project the building design over whole project lifecycle [3]. This is based upon the concept of building information model, as discussed below.

Building information model is a computer model database of building design information, which also contains information about the building's construction, management, operations and maintenance [3, 4]. The concept evolved with the introduction of 'object' (such as walls, roofs, doors and windows) oriented CAD, which contains both graphical (i.e. drawings) and non-graphical (e.g. specifications and schedule) data of the building in a logical structure, forming a highly coordinated repository. Changes in each item are made at only one place, and all project participants see the same information. This allows increased communication, considerably reduces time and cost, and avoids many potential disputes.

3 THE SETTING FOR BIM

Project Documentation in traditional construction contracting occurs with 2D drawings and specifications, which serves as the main mode of communication

between many '2 parties', e.g. client and consultant, client and contractor, consultant and contractor, and contractor and subcontractor. During each communication, parties have 3D visualization in mind with 2D documents, which may be correct or incorrect, and the 'issuing party' is not always physically present for clarifications. Moreover, many changes occur to those 2D drawings during the project progress through subsequent multiple edits. Such changes may originate from diverse experts and consultants, and consequent changes are made in isolation, which may have chain reactions. Some of the design parameters may lead to conflicting social, economic and legislative constraints, where a balance needs to be maintained. Furthermore, step by step adjustments to 2D documentation are laborious, time consuming, costly and may be erroneous. They are highly difficult to coordinate for the client too. BIM can help in such changing and adapting the design, planning schedules and cost estimates to aid client decision-making.

4 WHAT BIM CAN DO?

BIM can help in meeting goals for process improvements, productivity enhancement, and sustainable construction. For example, BIM can help:

- full scale analysis of passive design issues, e.g. relating to geography, climate, place, surroundings systems and resources [5, 6];
- to efficiently consider various aspects of energy use, emission of GHG or CO_2, waste generation, life cycle cost, and facilities management, and thereby improve sustainability rating [6];
- to reduce planning time and insurance cost, and improve project quality, risk management and life-cycle performance [7];
- to consider innovative ideas and adopt best practices in construction, e.g. lean construction and prefabrication [8];

Thus BIM can play a significant role in delivering construction projects and improving the efficiency and effectiveness of the integrated design and construction process. The BIM process can conduct a series of 'what-if' analyses to simulate and compare the impacts of different variables through the whole life cycle of the buildings / projects for a range of trade-offs, such as: predict & plan the construction process, determine cost options, maximise sustainability, investigate energy requirements, examine accessibility, determine maintenance needs, incorporate crime deterrent features, examine the building's acoustics, etc. The eventual prime benefit of BIM process is to develop project specific multi-dimensional and fully functional (building information) model (Figure 1), which can be used during the construction of the project, through to operation phase, e.g. in repair and maintenance, and finally to the demolition of the structure.
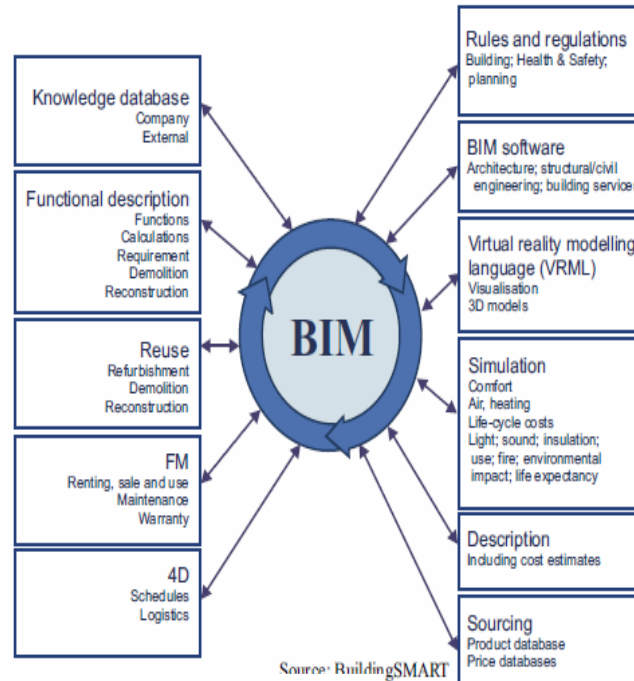
Figure 1: Project specific building information model [9]

5 WHAT NEEDS TO BE DONE?

Clearly, there exists an array of barriers to adopting BIM, e.g. skills and capability development, setting standards for various software, inter-operability issues, and cultural resistance of the competing contract parties, just a few to mention [7]. However, probably the most important aspect of BIM hinges around the teamwork based work environment that supports inputs from, and collaboration of, all major contract parties. A suitable procurement strategy seems to empower BIM adoption, by allowing effective collaboration between contract parties, e.g. in terms of information sharing, joint decision making, risk management, and equitable sharing of any pains or gains. Ideally, the procurement strategy should allow sharing of information, and inputs from all contract parties starting from the preconstruction stage, for effective examinations of alternatives and joint decision making and design. As such, the rest of this article examines the nature of 'information sharing' between the contract parties and 'workflow' within the available four broad types of procurement strategies, namely design-bid-build, design and build, management oriented approaches, and integrated delivery approaches. Information sharing and workflow are examined in the context of five categories: preconstruction, communication and collaboration methods, types of documents, clarification of information, and project closeout [5].

6   INFORMATION AND WORKFLOW

6.1   Design-bid-build (DBB) procurement strategy

Design-Bid-Build (DBB) type of procurement is characterised by separate and sequential activities of designing by consultants, bidding by clients or their representatives, and building by contractors. No information is shared between the consultant and contractor during design stage. Documentation comprises no digital information, but 2D drawings and specifications in hard copies, PDF format, or CAD images. Collaboration takes place, if there is any, only during construction stage, when all the planning and design documentation have been finalised. *Takeoff* is done manually or with the help of digitiser, requiring clarifications. Addenda are issued using supplemental drawings, which also require clarifications. All these are time consuming to do and also lack accuracy. Hard copies of original documents, along with addenda or 'as-built' drawings, and O&M manuals are handed over at the closeout. Thus, it seems not suitable for BIM.

6.2   Design-build (DB) procurement strategy

Under DB strategy, client prepares an initial design, which is then passed to DB team at preconstruction stage, who develops the full design and executes the construction [10]. So, a single entity streamlines the information both in design and construction phases. Communication occurs at much earlier stage (compared to DBB) when the client hands over the initial design to the DB party. This is also the time when collaboration begins between DB team and client. DB team starts with partial documentation from the initial design, gradually develops the design using the information already passed to them or by enquiring the client and simultaneously carry out construction. Thus, communication and collaboration take place both in construction and design processes, and client and DB party.

   Although the similar types of documents (compared to DBB, i.e. PDF or CAD image) are exchanged, they occur with reduced formality. The DB team maintains a common digital file, which they do not handover to client. Clarification of information is relatively more than DBB, since performance specification (with initial design) is usually given to the DB team, any changes to which occur with cost updates. Documents handed over at project closeout are often of hybrid nature, i.e. in both paper and digital format (e.g. soft copy of PDF or CAD image) but without 'source' file. DB is thus seen to practice some aspect of BIM, e.g. information flow from client to DB team at much earlier stage, integration of design and construction process, potentially collaboration commences before design development, maintaining the same digital file both for the design and construction purposes, and handing over some digital file at project closeout. DB, therefore, may potentially give a good start to the clients towards using BIM.

6.3 Management oriented procurement strategy

Management oriented procurement strategies include: construction management (CM), management contracting (MC), design & management (DM), and CM-at-risk. Under CM approach, clients appoint a professional management consultant (i.e. construction manager) to programme and organise all the works of design and construction into a series of packages, by different design team and works contractors, where construction manager does not become any party to any works contracts [11]. However, the contractor is selected at an early project stage in MC approach, for his input into design on constructability and construction methods, and to manage the construction process. The management contractor does not usually carry out any construction work himself, instead the work is divided into convenient packages to tender separately to subcontractors [12]. Under DM approach, consultant or designer designs the project, and supervises the construction works for client. Under CM-at-risk approach, construction manager acts as consultant to client at development & design stage for design-documentation, and as general contractor at construction phase. Projects are usually delivered with GMP (guaranteed maximum price) basis. This allows early involvement of contractors / subcontractors in design and documentation, and all parties to have a stake in the project development [5].

Since the same construction manager acts both as contractor and consultant, there is a continuous flow of information between contractor & consultant, as such contractor continuously updates the design team of cost and other consequences on the basis of 'current' documentation. This allows better collaboration between client and construction manager. However, the arrangement allows the contractor to enter into the realm of client and design programme management, which may create fear to client that the contractor is taking too much control of the project. As such a balance between information flow, workflow, collaboration and management of the project needs to be maintained. Nevertheless, the information flow and the collaboration help to develop a single model of the project (e.g. in PDF or CAD), starting from the project development and to the construction phase, which may be distributed / shared by rapid transfer methods, e.g. using email or project FTP (file transfer protocol).

The project experiences integration at preconstruction stage and the whole team focuses on achieving project objectives. Any clarification at preconstruction stage is given by direct interaction and input from contractors and subcontractors. During bidding stage, designers and contractors supply maximum information to their respective subcontractor, whereas contractors usually mediates among the subcontractors during construction stage, since profitability is tied up with contractor's performance and project coordination. Documents handed over at project closeout are similar to other methods, but sometimes facility manager is brought to define closeout deliverables.

6.4   Integrated procurement strategy

Integration in construction may be summarised as a process that integrates people, systems, business structures and practices; harnesses collaboration of all parties; reduces all kinds of wastes; and optimises efficiency through all project phases of design, fabrication / documentation and construction. Integration in construction is frequently compared to 'vertical integration', where contract parties work and collaborate in such a way that, as if, they belong to a single organisation [13].

Integrated procurement strategies, with the help of recent technological developments, allow such integration of team members from the beginning of the project (i.e. very early preconstruction stage) [7]. In terms of communication, everybody works on the same platform and shares the same information, which allows seamless collaboration between the parties and sharing risk and reward in an agreed incentive scheme. Documents include both individual and professional focussed models, for which a change to one element will have changes everywhere. Team members may seek and clarify various information continuously to each other, as they all freely share and use the information from the same database. Stakeholders have their say, but eventually informed decisions are taken as a whole and to benefit the project. Facility manager is involved during design, construction, as well as in preparing the project closeout documents, since the same design and model prepared for the project to be used to maintain the facility. Various editable documents, data and tools come in usable format than CAD.

7   CONCLUDING OBSERVATIONS

Recent technological imporvements appear to support the move for efficiency imporovement in construction. One such example is BIM, which can allow much advocated intrgation in construction, in the process of ensuring productitivity enhancements and implementing sustainable construction as well. However, BIM adoption requires the support of suitable procrement strategy. As such this paper presented an analysis of the available procurement strategies, in terms of their suitability to support BIM. It was seen than that traditional procurment strategy hardly can offer benefits to BIM. Design-build strategy offers the integration of design and construction process, while management oriented strategies (e.g. CM at risk) offers integration between design and construction processes, as well as between the relevant parties, along with their repective supply chains. However, integrated project delivery strategies seem to aptly contain and support BIM, in ters of process integration, collaborartion between the parties and in many more toher aspects. It was also observed that, suitability of the procrement strategies to support BIM increased as the collaborativeness of the strategies increased. So, integrated procurment stratgies are seen to empower BIM adoption in construction.

REFERENCES

[1] Lee, A., Marshall-Ponting, A.J., Aouad, G., Wu, S., Koh, I., Fu, C., Cooper, R., Betts, M., Kagioglou, M. & Fischer, M. (2003). *Developing a vision of nD-enabled construction*, Construct IT Report, ISBN: 1900491923

[2] Rischmoller, L., Fisher, M., Fox, R. & Alarcon, L. (2000). 4D Planning & Scheduling: Grounding Construction IT Research in Industry Practice. Proc. CIB W78 conf. Construction Information Technology: Iceland

[3] Lee, A., Wu, S., Marshall-Ponting, A., Aouad, G., Tah, J., Cooper, R., & Fu, C. (2005). *nD Modelling: a driver or enabler for construction improvement?* RICS research paper series, Volume 5, Number 6. ISBN 184 2192 000.

[4] Graphisoft, (2003) The Graphisoft Virtual Building: Bridging the Building Information Model from Concept into Reality. Graphisoft Whitepaper.

[5] Hardin, B. (2009). *BIM and Construction Management: proven tool, methods and workflows*, Indianapolis, IN: Wiley, ISBN: 9780470402351.

[6] Kilbert, C.J. (2013). *Sustainable Construction: green building design and delivery,* 3rd edition, Hoboken, NJ: Wiley. ISBN: 9780470904459.

[7] Hossain, M.K., Munns, A. & Rahman, M.M. (2013). "Enhancing team integration in building information modelling (BIM) projects". ARCOM Doctoral Workshop on BIM: Management and Interoperability, Edited by Prof David Boyd, 20 June, Birmingham City University, UK, 78-92.

[8] Rahman, M.M. (2014). "Barriers of implementing modern methods of construction". *J. of Management in Engineering*, 30 (1), 69-77.

[9] BuildingSMART (2000). *Constructing the business case: Building information modelling*. London: BSI. ISBN: 9780580709357.

[10] Rahman, M.M. (2003). *Revitalising Construction Project Procurement through Joint Risk Management*, Ph.D. Thesis, University of Hong Kong.

[11] Curtis, B., Ward, S. and Chapman, C. (1991). *Roles, responsibilities & risks in management contracting.* Construction Industry Research & Information Association (CIRIA), special publication 81, London, UK.

[12] Chappell, D. (1991). *Which form of building contract*, Architectural Design and Technological Press, London, UK.

[13] Rahman, M. M. and Kumaraswamy, M. M. (2012). Multi-country perspectives of relational contracting and integrated project teams. *J. of Construction Engineering and Management*, 138(4), 469-480.

MECHANISM OF ANCHOR TYPE RETAINING WALL IN BRACED EXCAVATION AND SIMULATION OF A FIELD OBSERVATION

H. M. SHAHIN[1], **T. Nakai**[2], **K. Okuda**[3] **and M. Kato**[4]

[1] Islamic University of Technology, Gazipur, Bangladesh
Email: shahin@iut-dhaka.edu

[2] Geo-Research Institute, Nagoya, Japan
Email: nakai@geor.co.jp

[3] Penta-Ocean Construction Co. Ltd., Miyagi, Japan

[4] Central Japan Railway, Gifu, Japan

Abstract. *In this research, a field observation of an anchor type retaining wall is simulated by finite element analysis. The finite element analyses are conducted with FEMtij-2D using an elastoplastic constitutive model named subloading t_{ij} model. For validating the results of the numerical simulation some laboratory model tests are carried out varying the length and number of anchors. Displacement of the retaining wall, tensile force of the anchors, and the ground movement are investigated. It has been revealed that longer anchor in the lower parts of the excavation produces a significant supporting effect resisting wall displacement of the backfill ground. The numerical analysis captures well the results of the field observation.*

Keywords: Anchor type retaining wall, Model test, Finite element Analysis, and Braced excavation.

1   INTRODUCTION

Usually open excavation causes problem to surrounding ground if the proper protection in deforming ground is not taken into account. Recently, anchors are used to excavate large section having deeper excavation depth. In present practical design method of retaining wall with anchor, earth pressure acting on the retaining wall and its stability as a whole are evaluated within rigid plasticity theory such as Rankine's earth pressure theory. The wall deflection is usually calculated using the beam spring model with Rankine's earth pressure theory, in the same way as that of the retaining wall with struts. In the literature [8], it is found that anchored wall has the restraining ability of wall movement greater than that of the braced wall, which emphasizes the necessity of investigating the mechanism of anchored wall.

In this paper, a field observation of an anchor type retaining wall is simulated by finite element analysis after validating the results of the numerical simulation corresponding to some model tests for the mass of aluminum rods. In the first part, the mechanism of anchor type retaining wall by model tests and the validation of corresponding numerical analyses is investigated. In our previous researches [2] and [5], investigation on the deformation mechanism of the ground has been done considering strut-type retaining wall. The same constitutive model named as subloading t_{ij} model [1] and the same sets of parameter are used in this research. This model can describe typical stress deformation and strength characteristics of soils such as the influence of intermediate principal stress, the influence of stress path dependency of plastic flow and the influence of density and/or confining pressure.

2   2D MODEL TESTS AND NUMRICAL SIMULATIONS

2.1   Outline of 2D Model Tests

Figure 1 shows a schematic diagram of the two-dimensional apparatus. The details of the model tests have been illustrated in the reference [7]. The size of the model ground is 680mm in width and 450mm in height. Aluminum rods of 5cm in length, having diameters of 1.6mm and 3.0mm and mixed with the ratio of 3:2 in weight, are used as the model ground (unit weight of the mass is 20.4kN/m^3). The retaining wall is 300mm in length, 60mm in width and 0.5mm in thickness, which is a plate of aluminum material. In the experiment the model ground was excavated with a layer of 15mm in thickness up to a possible depth of excavation. Pre-stress is applied at the head of each anchor. The anchor is modeled connecting the head and the anchor plate by a piano wire (thread) at both sides of the ground. By taking photographs with a digital camera and using PIV technique the ground movements and consequently the deviatoric strain distribution in the ground is captured. The wall deformation is also measured using digitizer from the photographs of the ground.
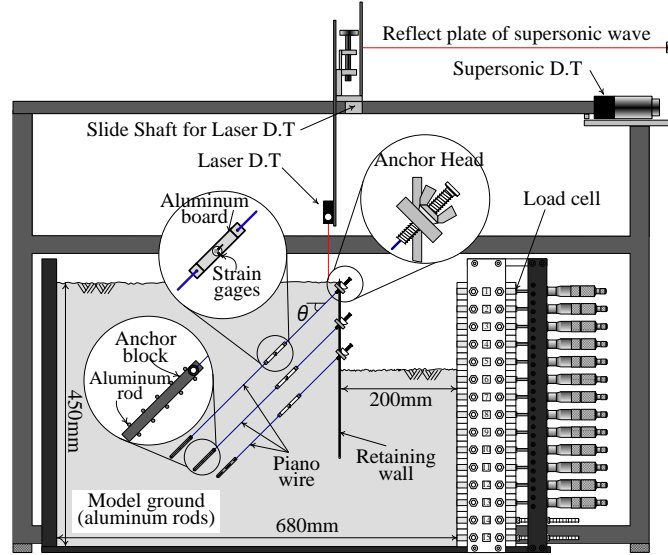
Figure 1: Schematic diagram of the apparatus.

Table 1: Test Patterns.

Test		Anchor length (mm)			Sheet pile length (mm)
		L_1	L_2	L_3	
Series 1	S1-C1	150		-	300
	S1-C2			100	
Series 2	S2-C1	300	125	100	
	S2-C2			300	
Series 3	S3-C1	150		100	240
	S3-C2			150	

Table 1 shows the experimental pattern. In the table, L_1 is the length of the upper anchor; L_2 and L_3 are the lengths of the middle and lower anchor, respectively. Excavation depth during the installation of the 1st stage anchor is 30mm, the 2nd stage anchor is 90mm and the 3rd stage anchor is 150mm. The anchor depth for the 1st stage anchor is 15mm, the 2nd stage anchor is 75mm and the 3rd stage anchor is 135mm from the surface of the ground. A plane of active earth pressure is assumed considering the final excavation depth of 210mm and an angle of internal friction of 30°. The anchor plate is setup outside of the assumed plane of active earth pressure. Series 1 deals with the number of anchors − two anchors are set in Case S1-C1 and three anchors are set in S1-C2. This series is considered as a basic pattern where the length of the upper anchor is 150mm, the middle anchor is 125mm and the lower anchor is 100mm (Case S1-C2). In Series

2, tests are carried out changing the length of the upper (S2-C1) and lower (S2-C2) anchors. In Series 1 and Series 2 the length of the sheet pile is 300mm. In Series 3, a shorter length of sheet pile (240mm) is used in the tests. The length of the anchors in Case S3-C1 is the same as S1-C2, and in S3-C2 the lower anchor is longer (150mm) than that of Case S3-C1. In the all tests, the inclination angle of the anchors is 30°.

2.2   Outline of Numerical Analyses

Figure 2 shows a typical mesh used in the finite element analyses for the simulations of the model tests. The analyses are carried out using finite element code FEMtij-2D developed in our laboratory using an elastoplastic constitutive model for soils, called the subloading t_{ij} model [1]. The sheet pile and anchor plates are modelled using elastic beam elements. The frictional behavior (friction angle $\delta=14^o$) between the sheet pile and the ground is simulated using elastoplastic joint elements. The anchor is modelled using truss element as it resists only tensile force. The excavation is simulated removing elements in the mesh corresponding to the excavation area of the model tests. The analyses are carried out with the same conditions of the model tests. The initial stresses of the ground are calculated by applying the body forces due to self-weight. The pre-stress is applied at the head of each anchor the same as the model tests. The same model parameters of the previous researches [3], [5] and [6] for the ground are used in this research.
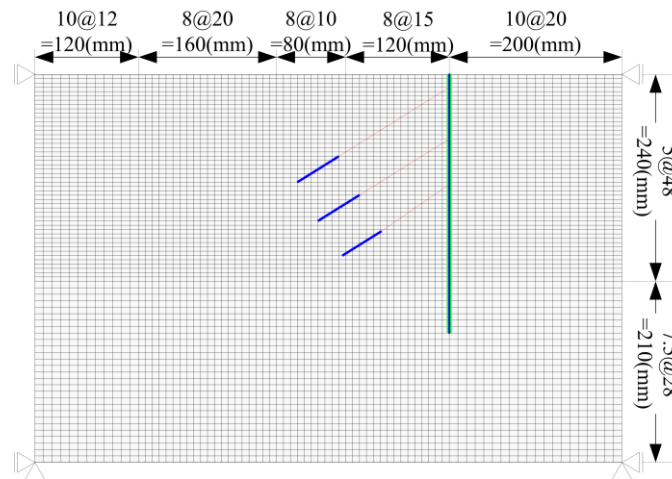

Figure 2: A typical mesh for finite element analysis.

2.3   Results and Discussions

2.3.1. Influence of Number of Anchors

Figure 3 shows the observed (Fig.3 (a)) and computed (Fig.3 (b)) wall displacements for different anchor lengths. The legend represents excavation depth (d). The arrows in the figures indicate the position of the anchors. It is revealed that the anchors restrict the wall displacement and surface settlement till the excavation depth of 150mm for both cases. When excavation depth exceeds 150mm a significant wall displacement is seen in S1-C1. The two-staged anchors (S1-C1) produces higher displacement in the ground than that of the three-staged anchors (S1-C2). The numerical simulations produce almost similar ground subsidence as the model tests.

Figure 4 illustrates distribution of shear strain of the model tests and numerical simulations. The distributions of shear strain of the model tests are obtained using Particle Image Velocimetry (PIV) technique. In the two-staged anchors the data is taken for the excavation depth of 195mm as the ground fails for further excavation. In the three-staged anchors the figure shows the results for the excavation depth of 210mm.
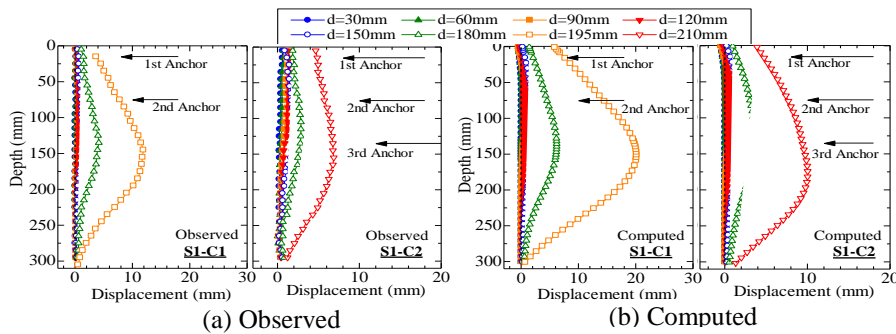

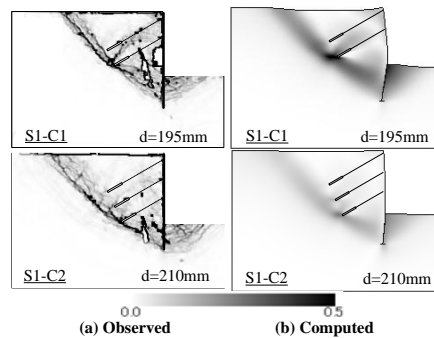Figure 3: Horizontal displacement of wall for different number of anchors.

Figure 4: Distribution of shear strain for different number of anchors.

The color contrast indicates the intensity of the shear strain. For both cases shear band develops outside of the anchor block. The numerical analyses well capture the observed wall displacement and shear strain distribution of the ground.

2.3.2. Influence of Anchor Lengths

Figure 5 shows the observed (Fig.5 (a)) and computed (Fig.5 (b)) wall displacements for different anchor lengths. It is revealed that the anchors restricts the wall displacement and surface settlement till the excavation depth of 180mm irrespective of the anchor length. When excavation depth exceeds 180mm a large wall displacement is observed near 150mm depth of the wall, and the surface subsidence increases significantly as well. For the excavation depth of 210mm, the influence of anchor length is seen remarkably. In Case S2-C2 (only the lower anchor length is longer) the wall displacement is smaller than that of Case S2-C1 (only the upper anchor length is longer). It is also seen that excavation up to 240mm is possible if the lower anchor is sufficiently longer. Therefore, if the lower anchor is longer, it is possible to make deeper excavation. The results of the numerical analyses show the same tendency of the model.

Figure 6 illustrates the shear strain distribution of the ground for this series. The figures show the results of the excavation depth of 210mm. It is found that in the case when only upper anchor is longer shear strain concentration in the shear band is almost similar to the test of S1-C2 (Fig.4). In contrast, longer lower anchor (S2-C2) significantly reduces shear strain in the ground. As the lower anchor is located outside the slip surface and produces sufficiently high pullout resistance it increases tensile force and hence a notable supporting effect can be speculated. Therefore, if the lower anchor is longer, it is possible to increase excavation depth. The results of the numerical analyses show the same tendency of the model tests.
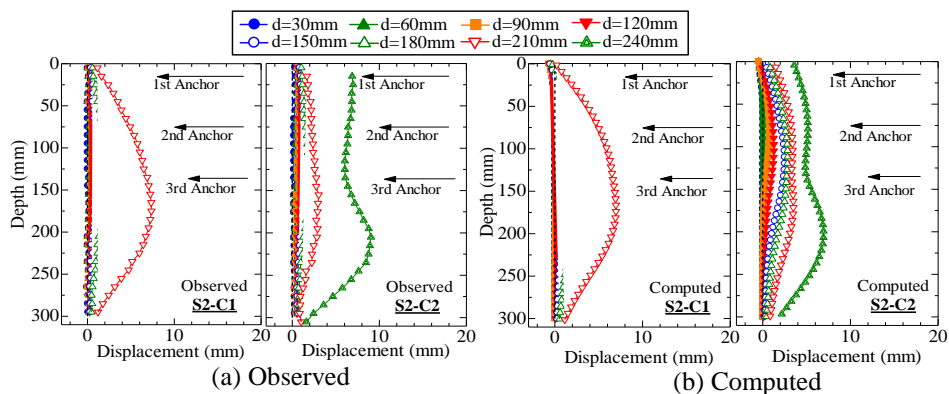

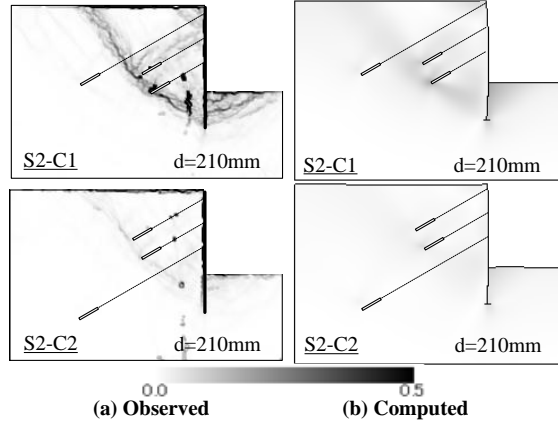Figure 5: Horizontal displacement of wall for different anchor lengths.

(a) Observed   (b) Computed

Figure 6: Distribution of shear strain: Series 2.

3   FIELD OBSERVATION AND ITS NUMERICAL SIMULATION

Figure 7 represents the geological condition, position of anchors and excavation produces of the field. Holocene layer and Pleistocene layer exist from the ground surface to the place near this monitoring site. Holocene layer is composed of a fine sandy layer (Aus), soft clay layer (Amc), and a sandy layer with medium density (As). On the other hand, Pleistocene layer exist in the lower part of Holocene layer, and is composed of a stiff clay layers (Tc), a dense gravel layer (Tg) and a dense sandy layer (Os).
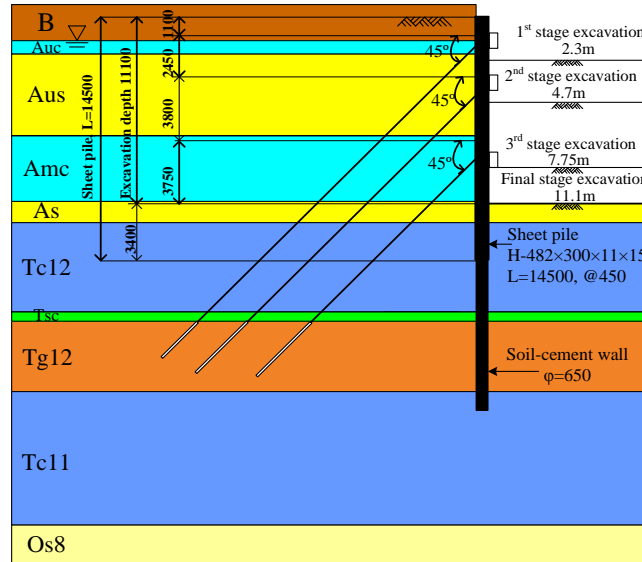

Figure 7: Dimension for numerical analysis of field.

Table 2 shows some parameters and characteristics of each layer. The excavation was carried out till the depth of 11.1m.

The length of the sheet pile was 14.5m, and below the sheet pile soil cement wall was placed till the Tc layer. The tip of the anchors was placed at Tg layer, the inclination angles of the anchors was 45°. Numerical analyses were conducted considering soil-water coupling condition as water table was near to the surface of the ground in the field.

Table 2: Parameters for field numerical analysis.

| Geological age	Layer symbol	Bottom depth (G.L.-m)	Parameters for FE Analyses							γ_t (kN/m^3)	k (cm/s)	SPT N
			λ	κ	ν	N	Rcs	β	a			
Man-made	B	-1.4	0.07	0.0045	0.2	1.10	3.2	2	30	17.0	1.67E-05	19
Alluvium layer	Auc	-2.2	0.16	0.02	0.2	1.23	2.1	1.3	500	17.24	1.67E-07	3
	Aus	-7.05	0.07	0.01	0.2	0.68	3.5	1.5	200	19.56	9.00E-04	3
	Amc	-10.95	0.16	0.02	0.2	1.23	2.25	1.57	40	16.09	1.67E-07	1
	As	-12.3	0.07	0.0045	0.2	1.10	3.2	2	30	19.40	2.80E-04	9
Diluvium layer	Tc12	-17.55	0.5630	0.00639	0.2	2.81	2.4	1.5	500	15.75	1.67E-07	5
	Tsc	-18.1	0.07	0.0045	0.2	1.10	3.2	2	30	20.80	8.90E-03	12
	Tg12	-22.3	0.07	0.0045	0.2	1.10	3.2	2	30	20.80	8.90E-03	56
	Tc11	-30.25	0.3255	0.01090	0.2	1.91	3.4	1.5	500	16.97	1.67E-07	9
Osaka layer	Os8	-40	0.07	0.0045	0.2	1.10	3.2	2	30	19.80	3.80E-03	49
	Oc	-50	0.6540	0.0170	0.2	3.23	3.4	1.5	500	15.42	1.67E-07	-
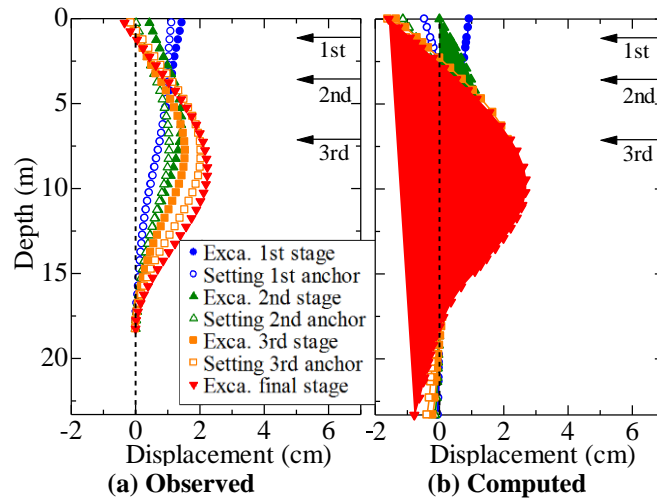
Figure 8: Observed and computed horizontal displacement of wall of the field

Figure 8 shows the observed and computed wall horizontal displacement. The maximum wall displacement after final stage of excavation is seen at the depth of about 10m. Figure 9 represents the observed and computed distribution of tensile

forces at the three anchors. It is found that tensile force of the 1st anchor decreases to some extent when the 2nd anchor is setup. The same tendency is also seen for the 2nd anchor when the 3rd anchor is setup. The numerical analysis perfectly reproduces the wall displacement and tensile force of the anchors results of the field data.
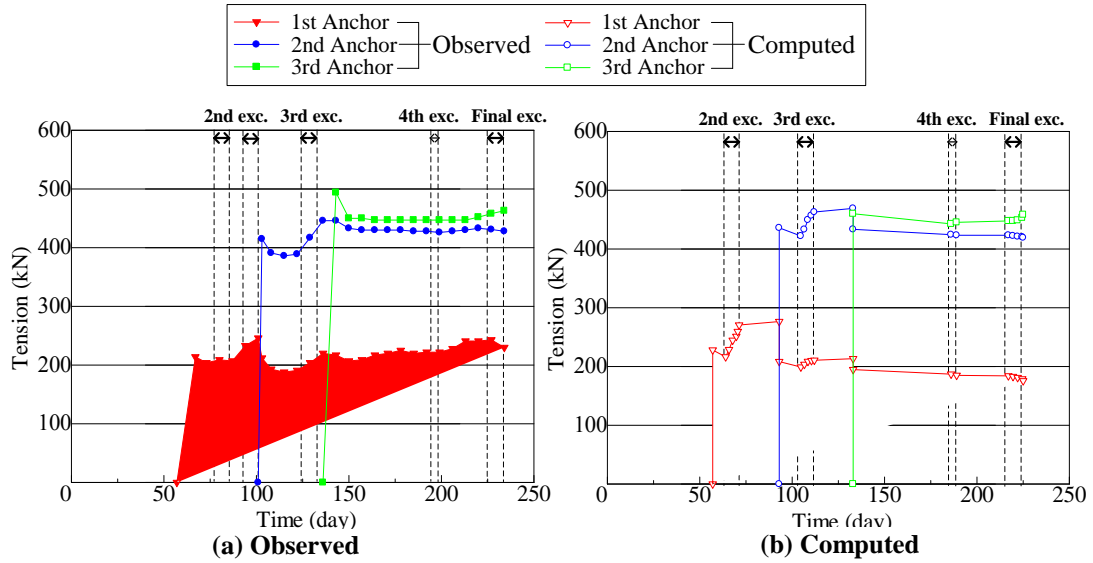

Figure 9: Observed and computed distribution of tensile force

4   CONCLUSIONS

In this research, two-dimensional model tests and the corresponding numerical analyses are carryout out on anchor type braced excavation. It is revealed that supporting effect of anchor in braced excavation can be achieved if the anchor block is setup outside the assumed slip surface developed during excavation. Especially, longer anchor in the lower part of the excavation produces a significant supporting effect resisting wall displacement and surface settlement of the backfill ground. As the wall deformation of the backfill ground increases with the advance of excavation it is important to install an anchor with a sufficient length in deeper excavation depth. It can also be concluded that the computed results in which typical stress-strain behavior of soils is appropriately taken into account agree well with the experimental results and observed field data qualitatively and quantitatively.

ACKNOWLEDGEMENTS

REFERENCES

[1] T. Nakai, M. Hinokio, 2004. A simple elastoplastic model for normally and over consolidated soils with unified material parameters. *Soils and Foundations*, **44(2)**, pp 53-70.

[2] T. Nakai, H. M. Shahin, N. Iwata, M. Ninomi, H. Takei, 2007. Influence of deflection process and mode of wall and existing building load on retaining wall. *Porc. of the 13th Asian Reg. Conf. on Soil Mech. and Geotechnical Engineering*, Kolkata, India, December, pp 481-484.

[3] T. Nakai, H. M. Shahin, Y. Morikawa, S. Masuda, S. Mio, 2014. Effect of reinforcement on bearing capacity of foundations, *Advances in Soil Dynamics and Foundation Engineering*, *GSP 240- ASCE*, pp 482-490.

[4] H. M. Shahin, T. Nakai, M. Kikumoto, Y. Uetani, F. Zhang, F. 2010. Interaction effect of retaining wall and existing foundations in braced excavation. *Deep and Underground Excavation, GSP 206 - ASCE*, pp 92-99.

[5] H. M. Shahin, T. Nakai, M. Kikumoto, Y. Uetani, 2011a. Influence of existing foundations on retaining wall in braced excavation. *Proc. of the 14th Asian Reg. Conf. on Soil Mech. and Geotechnical Engineering*, Hong Kong, May, pp 267.

[6] H. M. Shahin, T. Nakai, F. Zhang, M. Kikumoto, E. Nakahara, 2011b. Behavior of ground and response of existing foundation due to tunneling. *Soils and Foundations*, **51(3)**, pp 395-409.

[7] H. M. Shahin, T. Nakai, K. Okuda, M. Kato (2014): Support mechanism of anchor type retaining wall and influence of existing structure in braced excavation, Geomechanics from Micro to Macro, Cambridge, London, September, pp. 921-926.

[8] C.S. Yoo, 2001. Behavior of braced and anchored walls in soils overlying rock. *Journal of Geotechnical and Geoenvironmental Engineering*, **127(3)**, pp 225-233.

MECHANICAL PROPERTIES OF CNT REINFORCED COMPOSITE USING BERKOVICH NANOINDENTATION ANALYSIS

Khondaker S. AHMED[1], Ang Kok Keng[2] and Tahmida H. Shimu[3]

[1, 3] Department of Civil Engineering, Military Institute of Science and Technology, Bangladesh

[2] Department of Civil & Environmental Engineering, National University of Singapore, Singapore

Email: [1]drksa@ce.mist.ac.bd and [2]tahmida@ce.mist.ac.bd

Abstract. *Spherical and Berkovich indentation tests are carried out numerically using finite element method for uniformly dispersed Carbon Nanotube (CNT) in polymer matrix in which perfectly bonded CNT/matrix interface is considered. Large strain elasto-plastic analysis is performed to investigate the actual scenario of nanoindentation test. This study investigates how addition of CNT in polymer matrix influences the mechanical properties like hardness, elastic modulus of nanocomposite. Since the wall thickness to radius ratio (t/r) is significantly small for SWCNT there is a huge possibility of lateral buckling which is a function of the location of indentation tip as well as the mechanical properties of matrix. Separate finite element models are constructed to compare the result with Berkovich indentation. This study also investigates the buckling behavior of different nanotube in different polymer matrix.*

Keywords: Carbon nanotube, Nano-indentation, Elasto-plastic, Finite element model.

1 INTRODUCTION

Mechanical properties like modulus of elasticity, hardness or co-efficient of friction at the fibre/matrix interface of composites are some of the key features that are essential to determine before their application. It becomes more crucial to predict those properties using numerical methods for nanocomposite for which experimental set-up is quite difficult and sometimes impossible. The elastic modulus can be determined through a procedure originally proposed by Loubet et al. [4] and by Doerner and Nix [5] and subsequently developed by Oliver and Pharr [6]. It is based on the elastic analysis that is conducted by the contact of a punch with a semi-infinite space proposed by Sneddon [7]. In the analysis, it is assumed that the area of contact between the indenter and the specimen remains constant when the unloading stage begins. The gradient of the load-indentation curve during unloading is given by the following relation

$$S = \frac{|dF|}{|dh|}\bigg|_{h=h_t} = \alpha E_{ef} \sqrt{A_p} \tag{1}$$

Where,

S	represents Contact Stiffness
h_t	is the total indentation depth
A_p	the projected area
$\alpha = 2\sqrt{\pi}$	for Axisymmetric indenter
$\alpha = 1.167$	for Berkovich Indenter
E_{ef}	Effective Elastic Modulus
E_i	Indenter Elastic Modulus
E_f	Elastic Modulus of the Composite

The relationship between the indentation and the projected area of contacts expressed through the following equation

$$A_p = kh_p^2 \tag{2}$$

Where,

h_p	Effective indentation depth
$k = 24.5$	for Berkovich &Vicker Indentation

The hardness (H), being expressed as the ratio of the maximum applied load to the projected contact area, in the case of the Berkovich indenter, becomes equal to

$$H = \frac{F_{max}}{A_p} = \frac{F_{max}}{24.5 h_p^2} \qquad (3)$$

Research on indentation analysis shows that simulation of the indentation test through numerical analysis using finite elements allowed an increased under-standing of the process of deformation of the contact zone. Previously, like many research on indentation, a spherical indenter was considered in [10], Vickers indenter in [11] and a three-sided pyramid indenter in [12]. The results were used for identifying the stress strain curve of the material. In the analysis conducted in [12] considering two three-sided pyramid indenters with different inclination angles of the faces with respect to the load axis, the following relation was obtained as

$$\frac{H}{E_f} = 1.70 \left(\frac{\sigma_f}{E_f} \right)^{0.92} \qquad (4)$$

The inclination angles of the faces with respect to the loading axis were 65.3^0 and 35.3^0, in the first case the indenter is known as Berkovich, while in the second as 'cube corner'. Expressing the constitutive relation of the material by the Ramberg Osgood law gives

$$\varepsilon - \frac{\sigma}{E_f} = \frac{\beta}{E_f} \sigma^n \qquad (5)$$

Where,

$\varepsilon - \dfrac{\sigma}{E_f}$,   represents Plastic Strain

n is the strain hardening coefficient

β Characteristics constant of Material

The Equation can be rewritten as

$$\sigma = K \left(\varepsilon_p \right)^m ; \quad K = Y \left(\frac{E}{Y} \right)^m ; \quad K = \left(\frac{E}{Y} \right)^{\frac{1}{n}} \qquad (6a-c)$$

2   FINITE ELEMENT MODEL

Initially, an axisymmetric finite element model has been developed to investigate the mechanical properties of nanocomposite in which perfectly bonded CNT/matrix interface is considered. In the model, nanotubes are considered to be homogeneous solid and uniformly dispersed in both directions. Investigations are conducted for both thick-walled (thickness 0.34nm) and thin-walled nanotube (thickness 0.066nm). Outer radiuses of the CNT are taken to be 1nm. Since the fibre strength is much higher than the matrix, more finer mesh is considered at the CNT/ Matrix interface. In addition, a bias ratio of 10 is used to make the matrix more finer near the indenter tip. The typical FE model for thin walled nanotube is presented on the left side of Fig.1. The axisymmetric model for nano composite considering thick walled nanotube as well as meshing is presented on the right side of Fig.1.In this study, both spherical and Berkovich indentation analysis are conducted for both thin walled and thick-walled carbon nanotubes.

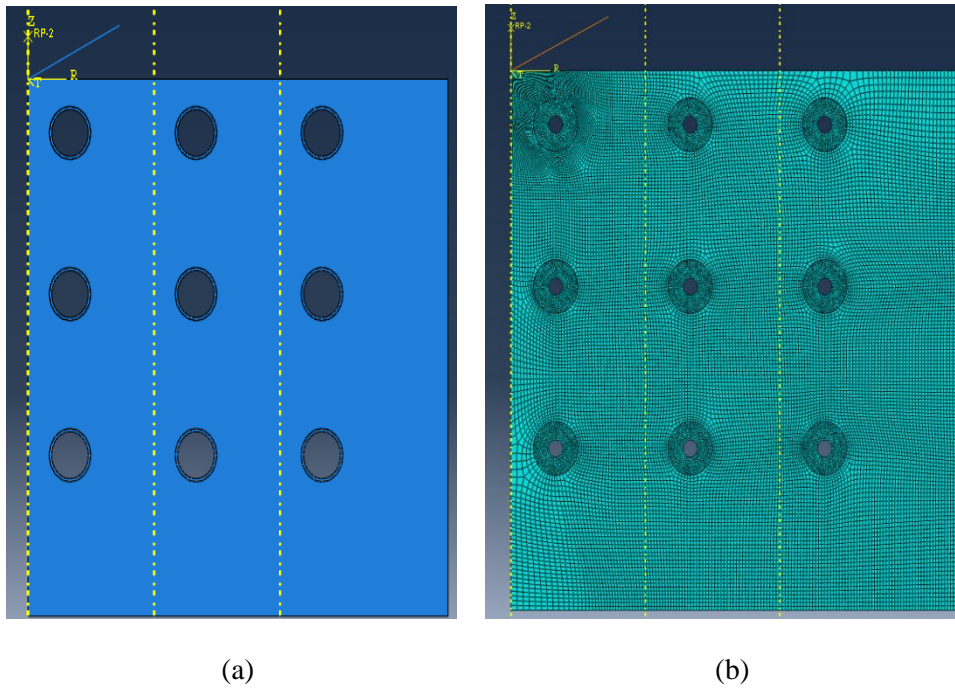(a)   (b)

Figure1: FE model for CNT in polymer composite (a) thin walled & (b) thick walled

3   RESULT & DISCUSSION

After successfully modeled the nanocomposite for different type wall thickness and different indenter, key results are presented. In order to investigate the influence of nanotube in polymer composite, a force displacement curve for pure epoxy and 1.3% thin walled CNT in matrix is presented in Fig.2. The figure shows a comparison of force/displacement relationship between CNT (1.3% by volume) reinforced epoxy composite and pure epoxy matrix.
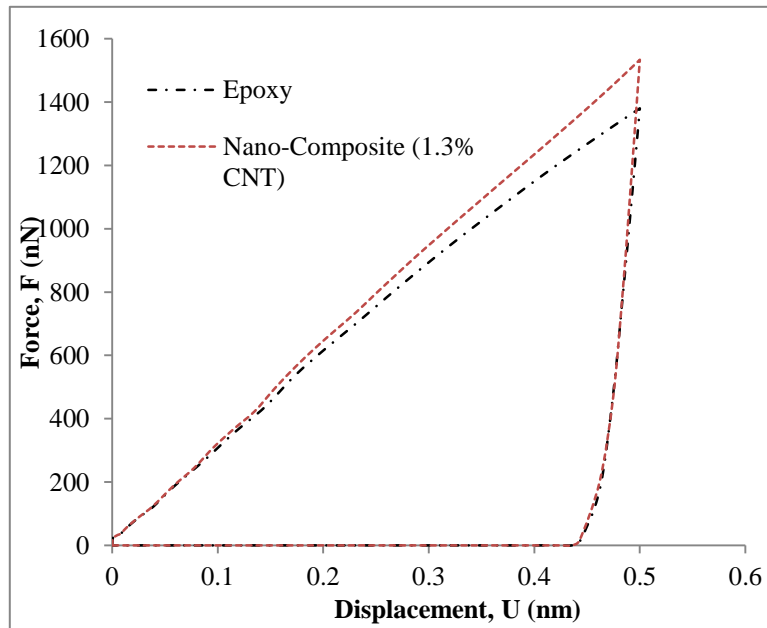

Figure 2: Force/displacement relationship for Nano-composite pure epoxy matrix

Both of the relationships curves show that with the increase of indentation displacement, force also increase nearly in linear pattern. It can also be seen from the figure that with the addition of carbon nanotube in epoxy matrix, required indentation force increases corresponding to the same displacement. The maximum required forces for 0.50nm indentation depth are found to be 1533 nN and 1320 nN for nanocomposite and pure epoxy, respectively. The slope of the force displacement curve for nanocomposite is higher than that of the epoxy for the cases of both loading and unloading. Therefore, it can be concluded from this result that the modulus of elasticity of epoxy increases (17%) significantly with the addition of CNT which in fact reflects the reinforcing potential of CNT in polymer matrix.

Result of nano-indentation simulation for thick walled carbon nanotube is presented in terms of stress distribution in Fig.3. The bekovich simulation result shows that the higher stress is developed near the indenter tip as expected. In addition, maximum stress is developed in the CNT compare to the corresponding matrix region. It is interesting to note that though the indenter tip displaced downward inside the matrix, the shape of the thick-walled tube remains unchanged. The shape of the stress distribution suggests that the stress flow is higher in lateral direction than the vertical.

Spherical indentation simulation of thin walled carbon nanotube is presented in Fig.4. The stress distribution of the nano-indentation shows that the maximum stress is developed in the tube located near the indenter tip. It is important to observe that the shape of the thick-walled tube changes as the indenter tip displaced downward inside the matrix.
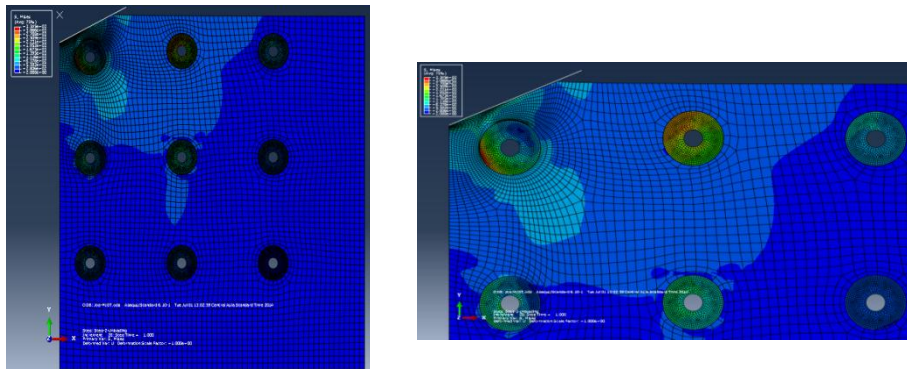
Figure 3: Stress distribution for Berkovich indentation of thick-walled CNT in nanocomposite
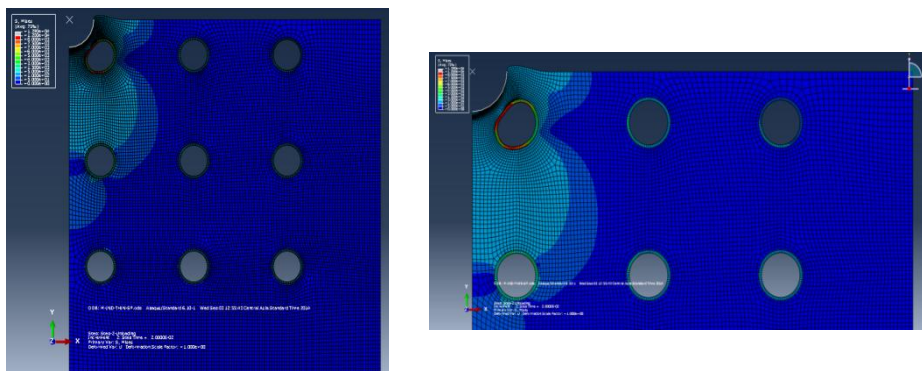
Fig. 4: Stress distribution for spherical indentation of thin-walled CNT in nanocomposite
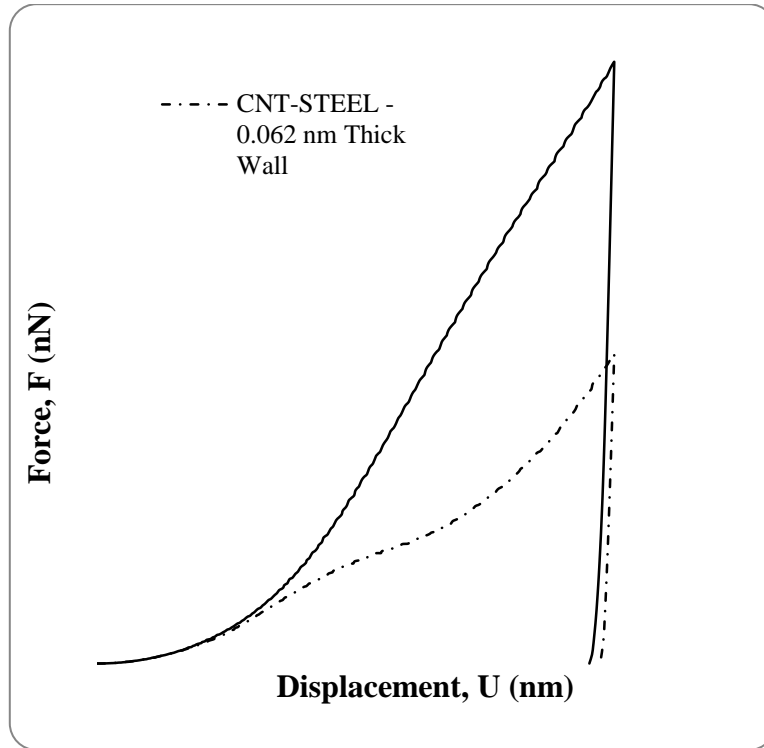
Figure 5: Wall Thickness dependency of CNT-Steel nanocomposites

Figure 5 shows a comparison of force displacement relationship of CNT steel nanocomposite for different wall thickness of CNT. In this study a comparison has been made for thin (0.062nm) and thick (0.34nm) walled CNT with the same diameter of CNT in steel matrix. The figure shows that there is no significant difference in forces up to 0.25nm indentation depth. However, the required force sharply increases for 0.34nm thick CNT-Steel composite particularly after 0.30nm indentation depth. On the other hand, the force increment of thin walled CNT-Steel composite is not linear and the difference with thick walled CNT-Steel composite is very significant. Therefore, the maximum required force for 0.788nm indentation depth is very much higher for thick walled CNT reinforced steel composites. This phenomenon of the CNT reinforced composite can be explained as with the increase of indentation depth the thin walled CNT starts to buckle where the thick walled CNT remains same as given in Figure 4.
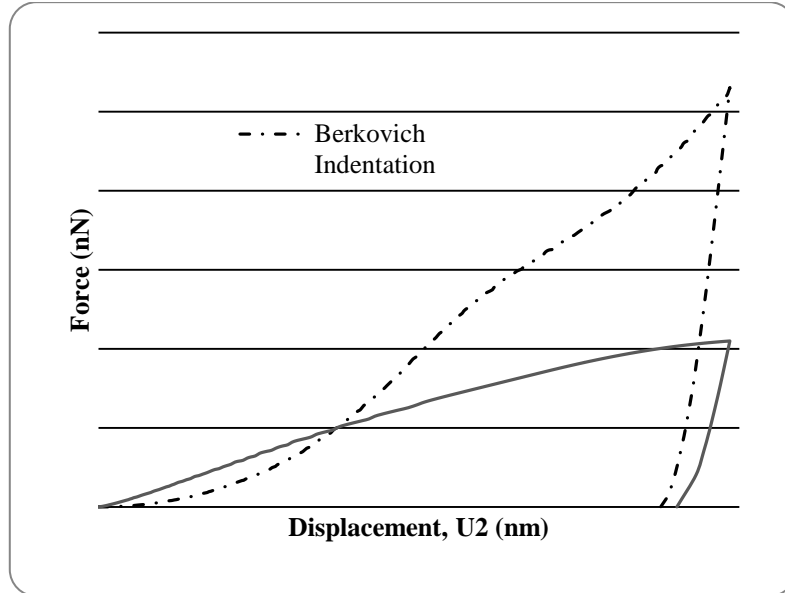
Figure 6: A comparison in terms of force-displacement relationship between spherical and Berkovich indentation

Force displacement relationship for spherical and Berkovich indentation analysis are presented and compared in Fig.6. It can be seen from the figure that maximum stress is larger for Berkovich indentation than that of spherical indentation. This phenomenon is expected since total surface area covered by Berkovich indenter is larger than that of spherical indenter. Plastic behavior of the nanocomposite is found to be higher in case of Berkovich indentation since residual displacement is higher after unloading. It is also important to note that their force displacement profiles do not match with each other. Therefore, it can be concluded that the indentation analysis is largely dependent on the type indenter particularly their force displacement profile.

4   CONCLUSION

Several finite element models have been developed to investigate Spherical and Berkovich indentation tests for uniformly dispersed Carbon Nanotube in polymer matrix in which perfectly bonded CNT/matrix interface is considered. The model shows that the CNT experiences significantly larger stress compared to matrix. It is also found that the nanotube starts to buckle in the polymer matrix when thin walled CNTs are used. Subsequently, smaller indentation force is found for thin walled tube compared to the thick walled carbon nanotube. This can be explained by the fact that the thin walled carbon nanotube starts to buckle and results

smaller force. A comparison between Berkovich and spherical indentation analysis has also been conducted to observe the indenter dependency in force-displacement profile of the nanocomposite. The results shows that the profiles are quite different and does not match with each other which can be explained as the surface area for Berkovich indenter is much larger than that of the spherical indenter. Therefore, this study may contribute in designing future carbon nanotube reinforced nanostructure where experimental study is very difficult to conduct.

REFERENCES

[1] P. L. Larssont, A. E. Giannakopoulos, E. Soderlund, D. J. Rowcliffe, R. Vestergaard, 1996. Analysis of Berkovich Indentation. *Int. J. Solids Structures Vol. 33, No. 2,* Great Britain, pp. 221-248.

[2] S.S. Gupta, F.G. Bosco, R.C. Batra, 2010. Wall thickness and elastic moduli of single-walled carbon nanotubes from frequencies of axial, torsional and inextensional modes of vibration. *Computational Materials Science, Vol. 47, Issue No. 4,* pp 1049-1059

[3] Ashraf F. Bastawros (2006). Analysis of deformation-induced crack tip toughening inductile single crystals by nano-indentation. *International Journal of Solids and Structures, Vol. 43,* pp 7358–7370.

[4] Edy Harsono, (2009). Material characterization via simulated indentation test including effect of friction. *A PhD thesis submitted to Department of Civil Engineering, National University of Singapore.*

[5] S. Swaddiwudhipong, L.H. Poha, J. Huaa, Z.S. Liu, K.K. Tho, (2005). Modeling nano-indentation tests of glassy polymers using finite elements with strain gradient plasticity. *Materials Science and Engineering, A, Vol. 404* pp 179–187.

[6] Nima Nouri, Saeed Ziaei-Rad, Sara Adibi, Fathollah Karimzadeh, (2012). Fabrication and mechanical property prediction of carbon nanotube reinforced Aluminum nanocomposites. *Materials and Design, Vol. 34,* pp 1–14.

[7] Y. Kusano, I.M. Hutchings, (2003). Analysis of nano-indentation measurements on carbon nitride films. *Surface and Coatings Technology, Vol. 169 –170,* pp 739–742.

[8] L. De Fazio, S. Syngellakis, R. J. K. Wood, F.M. Fugiuele, G. Sciume´, (2001). Nanoindentation of CVD diamond: comparison of an FE model with analytical and experimental data. *Diamond and Related Materials, Vol. 10,* pp 765769

[9] Linmao Qian, Ming Li, Zhongrong Zhou, Hui Yang, Xinyu Shi, (2005). Comparison of nano-indentation hardness to microhardness. *Surface & Coatings Technology, Vol.195,* pp 264– 271.

[10] Helene Issele, David Mercier, Guillaume Parry, Rafael Estevez, Lionel Vignoud, Christian Olagnon, (2012). Determination of the Young's Modulus of a TiN Thin Film by Nanoindentation: Analytical Models and FEM Simulation. *e-Journal of Surface Science and Nanotechnology, Vol. 10 ,* pp 624-629.

[11] E. Harsono, S. Swaddiwudhipong, Z.S. Liu, (2009). Material characterization based on simulated spherical-Berkovich indentation tests. *Scripta Materialia, Vol.* 60, pp 972–975.